

AD-A055 857

FLORIDA STATE UNIV TALLAHASSEE GEOPHYSICAL FLUID DYN--ETC F/G 4/2
CLIMATE SIMULATION.(U)
MAR 78 R L PFEFFER

N00014-76-C-0844
NL

UNCLASSIFIED

1 OF 1
ADA
055857



END
DATE
FILMED
8-78
DOC

ADA
558

FOR FURTHER TRAN

1
B.S.

AD A 055857

AD No. _____
JDC FILE COPY

9 FINAL REPORT

on

6 Climate Simulation

15
ONR Contract N00014-76-C-0844 (NR 062-546)
N00014-77-C-0265
by

10 Richard L. Pfeffer
Principal Investigator
Geophysical Fluid Dynamics Institute
Florida State University

11 MAR 19 78

12 90p.

DDC
RECEIVED
JUN 19 1978
RESERVED

E

18 06 13 100

DISTRIBUTION STATEMENT A

Approved for public release
Distribution Unlimited

405 431

CL

PREFACE

Under contract N00014-76-C-0844 (NR 062-546) field distributions of fluid temperature and speed were measured in thermally-driven rotating fluids which simulate important aspects of meteorological and climatic atmospheric behavior. Climatic statistics were generated which have relevance to problem of extended range atmospheric prediction. The results of our experimental work and their interpretation are contained in two published papers which comprise this Final Report.

A. Cyclic Variations of the Imposed Temperature Contrast in a Thermally Driven Rotating Annulus of Fluid, J. Atmos. Sci., 35, 1978 by Buzyna, Pfeffer and Kung: This paper presents the results of an extensive series of experiments with periodic "seasonal" temperature changes superimposed upon otherwise known flows in the range of parameters pertinent to atmospheric weather and climatic variations. In these experiments the rotation rate (Ω) was held constant and the imposed temperature difference across the fluid (ΔT) was varied in a continuous, periodic fashion for up to 10 "years" after an initially stable climate was established. Whereas the flow in conventional annulus experiments was found to be *determinate* in the sense that it depended only upon the point in dimensionless-parameter space at which the experiment was conducted and the direction from which it was approached, the flow configuration in the experiments in which ΔT was varied cyclically was found to be *indeterminate* in the sense that it changed from one state to another sporadically and could not have been predicted solely as a function of "season". During different annual cycles the general circulation of the fluid in a particular season took on different behavioral characteristics. For example, the flow pattern which

18 06 13 100

developed in one summer season sometimes established itself and shaped events in the following winter season. Sometimes the patterns persisted into a third year before breaking into a new regime (e.g. wave number change, or change from amplitude vacillation to wave dispersion). This is similar to atmospheric events in which synoptic waves become established in different phases from normal, or in which the jet stream becomes established north or south of its normal position for considerable periods of time. Such abnormalities in the atmosphere are often accompanied by extended periods of drought, altered hurricane paths and/or early onset of winter conditions such as were experienced in recent winters. There are, of course, a number of feedback mechanisms at work in the atmosphere (including cloud and ice reflectivity, atmosphere-ocean interactions, mountain influences, etc). The fact that important similarities exist between atmospheric behavior and the behavior of fluids in rotating annulus experiments in which ocean, land and cloud irregularities are not present, however, emphasizes the fundamental role of the annulus model in studies of non-linear processes which shape climate and climatic changes.

B. Catastrophic Changes in Circulation Flow Patterns, American Scientist, 65 (5), 614-621, 1977 by Lacher, McArthur and Buzyna: One by-product of our "seasonal" experiments was the observation that strong hysteresis effects are present when the imposed ΔT is varied very slowly. In particular, certain wave number changes take place at different points in dimensionless-parameter space depending upon whether ΔT is slowly increased or decreased. This phenomenon is one which was reported on earlier by Fultz and others.

In our laboratory we have conducted a series of such experiments with multi-probe temperature measurements and have determined the available potential energies associated with the two states possible at each of several points in dimensionless-parameter space. The important dimensionless parameters for these flows are the thermal Rossby number (ratio of inertial to Coriolis acceleration), the Taylor number (square of the ratio of the Coriolis acceleration to the viscous force) and the Prandtl number (ratio of the viscous to the thermal dissipation coefficient). We found that depending upon the direction from which a point in dimensionless-parameter space was approached, different energy levels exist. This led to the paper by Lacher, McArthur and Buzyna in which they presented an alternative method of representing bimodal hysteresis phenomena using Thom's catastrophe theory (see his book entitled "Structural Stability and Morphogenesis" Reading MA: W. A. Benjamin Inc. 1975). The model proposed is the simplest possible model for describing hysteresis and intransitivity phenomena observed in laboratory experiments displaying abrupt climatic changes. The behavior of the fluid in such experiments is found to be closely approximated by a cusp model of the form

$$\dot{E} = f(\Omega, \Delta T, E)$$

where E is a measure of the available energy in the system, \dot{E} is the time rate of change of E , Ω is the rate of rotation of the system and ΔT is the imposed "pole to equator" temperature difference. The function f is the gradient of a potential function whose qualitative properties are not changed by small perturbations. A reprint of this paper with further details is contained at the end of this Final Report.

1. Introduction

The earth's atmosphere is subjected to periodic thermal forcing with a cycle period of 365 1/4 rotations. While variations of the zonally-averaged temperatures in the tropics are small, arctic and mid-latitude temperatures undergo marked seasonal oscillations. In winter, when arctic temperatures are lowest, intense baroclinic disturbances are in evidence over the hemisphere and the hemispheric average eddy available potential and kinetic energies reach their peaks. In summer, the eddy energies reach their lowest magnitudes. It is not obvious, a priori, whether more intense synoptic wave activity is universally associated with greater thermal forcing, or whether this result is a peculiarity of the earth's atmospheric circulation due to the particular rate of rotation of this planet and the range of intensities of the thermal forcing to which it is subjected. Indeed, laboratory experiments and baroclinic theory reveal that synoptic waves are replaced by symmetric flow when the imposed thermal forcing exceeds a certain critical magnitude.

In spite of the periodic nature of the thermal forcing function, the scale, phase and propagation speed of the synoptic disturbances display intra-annual differences which, in turn, are accompanied by rather significant differences in weather phenomena in the same season of different years. It is recognized, in this connection, that the earth's atmosphere

is also subjected to geographically irregular thermal and orographic influences and that it participates in a complex set of feedback mechanisms involving releases of latent heat of condensation and sublimation, exchanges of heat with the oceans, cloud and ice reflectivity, etc. At present, it is not yet known to what extent intra-annual differences in weather patterns are attributable to the complexities of the forcing functions and feedback mechanisms, and to what extent they are inherent in the system due to the non-linear property of hysteresis ("memory").

It is the purpose of the present article to explore answers to such questions using a laboratory experimental model of a rotating fluid subjected to periodic thermal forcing. The dimensionless parameters of the model are controlled such as to produce quasi-geostrophic, quasi-non-divergent, strongly stratified flow similar to that in the earth's atmosphere. The model is, however, by design, devoid of many of the complexities of the atmospheric forcing function and of the feedback mechanisms to which the atmosphere is subjected.

Snyder and Youtz (1969) have made a limited study of the behavior of such a fluid subjected to a sinusoidally varying imposed temperature contrast in a region of dimensionless-parameter space centered on the static transition between wave numbers 2 and 3. The region in which their experiments were conducted displayed weak hysteresis properties. With roughly a 30% variation around a nominally 10°C imposed temperature

contrast, they found that, in the limit of slow cycling, transitions between wave numbers 2 and 3 tended to take place near the mean value of the imposed temperature contrast for such transitions under static conditions. With decreasing cycle period the transition points deviated increasingly from the static value until, at sufficiently small cycle periods, no transition took place.

In the present study experiments were conducted at three different rotation rates, with four different ranges of variation of the imposed temperature contrast, and with four different cycle periods. Temperature spectra and eddy and zonal temperature variances were calculated and are presented in subsequent sections as a function of time. The region of dimensionless-parameter space in which these experiments were conducted displays strong hysteresis properties.

In order to provide a proper framework for interpretation of the results of experiments with periodically imposed thermal forcing, we shall review first some of the properties of thermally driven rotating flows which develop when the thermal driving force is not varied with time. We shall also examine the behavior of fluids subjected to small step changes of the thermal forcing function. Attention will be focused, in particular, on (1) the levels of thermal variance attained by different synoptic wave components at relevant points in dimensionless-parameter space, (2) the response time of the fluid to step changes in the thermal forcing function, and (3) the hysteresis characteristics

displayed when a point in dimensionless-parameter space is approached from different directions (i.e., by lowering or raising the thermal forcing function).

2. List of symbols and dimensionless parameters

R	radial distance from the axis of rotation to the annulus
z	height above the base of the fluid
t	time
a	radius of inner cylinder (7.303 cm)
b	radius of outer cylinder (14.923 cm)
H	depth of working fluid (15.0 cm)
\bar{T}	azimuthal ("zonal") average of the fluid temperature at a specified radius ("latitude")
T_i	inner bath temperature
ΔT	imposed temperature contrast between the inner and outer cylinders containing the working fluid
Ω	rate of rotation of annulus
g	acceleration of gravity
α	coefficient of volume expansion of the fluid
ρ	fluid density
ν	coefficient of kinematic viscosity of the fluid
k	coefficient of thermometric diffusivity of the fluid
$Pr \equiv \nu/k$	Prandtl number (57)
Ro_T	imposed thermal Rossby number $\{=g\alpha H\Delta T/[\Omega^2(b-a)^2]\}$
Ta	Taylor number $[=4\Omega^2(b-a)^4/\nu^2]$
V_z, V_E	zonal and eddy temperature variance, respectively, at mid-depth in the fluid

3. Apparatus and procedures

The working fluid used in this experimental series, 5 centistoke silicone fluid, depth 15 ± 0.05 cm, was contained in an annular region, the inner and outer radii of which were 7.303 and 14.923 ± 0.005 cm, respectively. The annular region was formed by two concentric brass cylinders of 0.43 cm wall thickness and 20.3 cm length imbedded in, and oriented normal to, a flat Plexiglas base 2.4 cm thick. The cylindrical walls were maintained at prescribed temperatures by means of circulating water baths in contact with the outside of the outer wall and the inside of the inner wall. The water in each bath was circulated at a rate of 2 gal. min^{-1} and its temperature was controlled to within $\pm 0.05^\circ\text{C}$.

The entire annulus assembly was mounted on a turntable with a hydrostatic oil bearing with its axis of symmetry concentric with the vertically-oriented rotational axis of the turntable. The turntable was driven by a direct-drive servo-controlled dc torque motor which provided long- and short-term rotational stability of the order of $\pm 0.01\%$. The axis of rotation was aligned within 5 sec of arc with the vertical (gravitational field).

The internal distribution of fluid temperature was measured with an array of bead thermistors positioned within the fluid by suspending them by their long leads (diam: 0.005 cm). The entire observational network embedded in the fluid consisted of a distribution of 14 single thermistors for temperature measure-

ments and 21 "quadruple" velocity-temperature transducers located at different depths and radii in the fluid as shown in Fig. 1. Each quadruple consisted of three bead thermistors forming an equilateral triangle in the horizontal plane which sensed the temperature field produced by a fourth heater bead located at the center of the triangle (as described by Fowles, Buckley and Ruppert, 1972). These were present in the fluid for the purpose of calibration and testing. Only temperature measurements were used in the present study. The total number of wires passing vertically in the fluid (including return leads) was 154. The details of the thermistor design and circuitry, the digital data acquisition system and the procedures used to extract and process the data are described by Pfeffer, Buzyna and Fowles (1974).

The cyclic variation of the temperature contrast (ΔT) across the annulus walls was accomplished by cycling the cold inner-bath temperature (T_i) while the warm outer bath temperature was maintained constant. A modified slider crank mechanism was used to produce a cyclic variation of the thermoregulator which controlled the cold bath temperature. In this version

the connecting link, of fixed length, was a string which wound around a shaft connected directly to the thermoregulator (mercury thermometer type with a rotating head). The turning of the thermoregulator varied the cold reservoir bath temperature in a cyclic fashion. The ratio of the distance between the thermoregulator shaft and the crank pivot to the length of the crank was 5.5. This combination gives a maximum

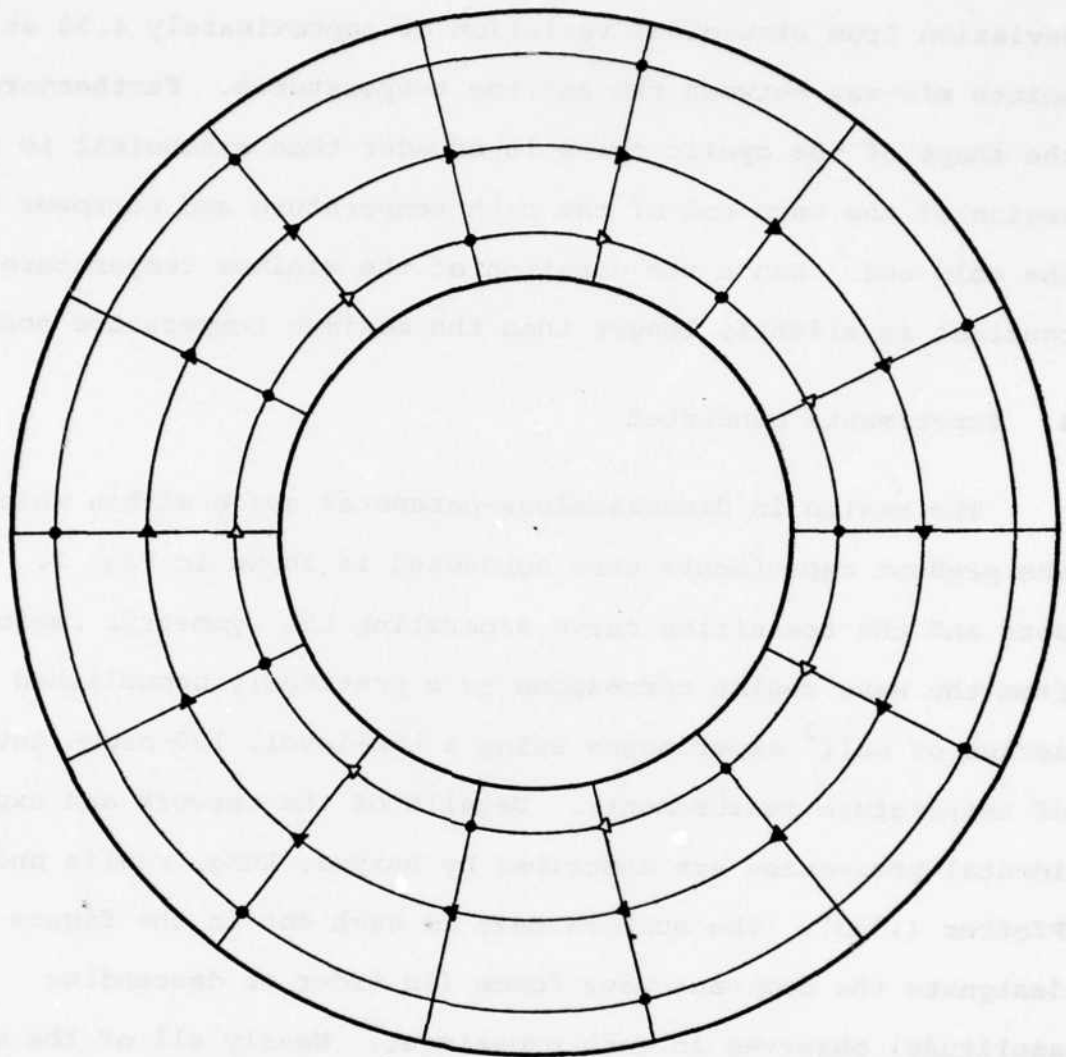


Fig. 1: Sketch showing horizontal distributions of thermistor probes at two levels in the annulus. The concentric circles represent radii $R = 8.57, 11.11$ and 13.65 cm ($1/6, 1/2$ and $5/6$ gap-width, respectively). The locations of single thermistors at mid-depth (7.50 cm from the base of the annulus) are designated by solid circles (●). The locations of "quadruples" (transducers consisting of four thermistors used for measuring fluid temperature and velocity) at 7.50 and 11.25 cm above the base of the annulus are designated by solid (▲) and open (△) triangles, respectively.

deviation from sinusoidal variation of approximately 4.5% at points mid-way between the extreme temperatures. Furthermore, the shape of the cyclic curve is broader than sinusoidal in the region of the warm end of the bath temperature and narrower at the cold end. Hence the duration of the minimum temperature contrast is slightly longer than the maximum temperature contrast.

4. Experiments conducted

The region in dimensionless-parameter space within which the present experiments were conducted is shown in Fig. 2. The dots and the transition curve separating the symmetric regime from the wave regime correspond to a previously unpublished series of null² experiments using a two-level, 100-probe network of temperature measurements. Details of the network and experimental procedures are described by Buzyna, Kung, Fowlis and Pfeffer (1973). The numbers next to each dot in the figure designate the dominant wave forms (in order of descending amplitude) observed in each experiment. Nearly all of the wave experiments exhibited some degree of amplitude vacillation of a single dominant mode, or of three adjacent dominant modes with different mean amplitudes and different magnitudes of vacillation. The single exception was an experiment designated in Fig. 2 by 4, 5, 6D which exhibited wave dispersion without significant variations in the amplitudes of the dominant waves. Three additional null experiments, indicated by crosses in Fig. 2, were

²Null experiments are defined here as experiments with the externally controlled parameters (rotation rate and imposed temperature contrast) held fixed.

conducted with the present observational network to help clarify the nature of the different wave states encountered in experiments with cyclic variations of the imposed temperature contrast. The control parameters and the associated dimensionless-parameters corresponding to these experiments are listed as experimental series G in Table 1.

Fig. 3 shows the magnitude of the time-mean eddy thermal variance of the fluid at the different points in dimensionless-parameter space at which null experiments with the earlier 100-probe network were conducted. Since imposed periodic fluctuations of the temperature contrast (ΔT) represent vertical paths in the Ro_T vs. Ta plane, it is clear by inspection of this diagram that whether or not the wave amplitudes will be larger in "winter" (high imposed temperature contrast) than in "summer" (low imposed temperature contrast) will depend upon where in dimensionless-parameter space the experiment is conducted. Judging by the observed behavior of the earth's atmosphere, it would appear that experiments C and D (Fig. 2 and Table 1) should be the most relevant of the present series, in this respect, to atmospheric seasonal changes.

In addition to the null experiments, experiment SE-32, series F (Table 1) was conducted to determine the response characteristics of the fluid to a near-step change in the cold-bath temperature (T_c) of 4.6°C with Ω held constant. In two other experiments in series F, SE-34 and SE-35, T_c was varied in smaller discrete steps over 16- and 24-hour periods, respectively.

TABLE I

experiment group, no.	ΔT (°C)	Ro_T	Ω (sec ⁻¹)	T_a (10 ⁷)	cycle period (hr)	($\partial \bar{T} / \partial z$) [*] (°C cm ⁻¹)
A 4	5.2 - 9.9	0.47 - 0.89	1.718	1.59	1 984.1	0.305
A 5	5.2 - 9.9	0.47 - 0.89	1.718	1.59	1 984.1	0.301
A 23	6.1 - 10.6	0.55 - 0.95	1.718	1.59	1 984.1	0.350
A 24	5.9 - 10.4	0.53 - 0.94	1.718	1.59	1 984.1	0.341
A 26	5.6 - 10.2	0.50 - 0.92	1.718	1.59	1 984.1	0.332
A 29	5.9 - 10.5	0.53 - 0.95	1.718	1.59	2 1968	0.340
B 31	7.8 - 10.0	0.70 - 0.90	1.718	1.59	0.5 492.1	0.361
C 33	1.3 - 5.7	0.12 - 0.51	1.718	1.59	1 984.1	0.162
D 22	5.5 - 10.1	0.27 - 0.51	2.304	2.86	1 1320	0.313
E 30	11.0 - 20.2	0.61 - 1.11	2.196	2.60	2 2516	0.590
F 32	5.9 - 10.5	0.53 - 0.95	1.718	1.59	- step -	0.337
F 34	6.1 - 10.6	0.55 - 0.95	1.718	1.59	16 15,747	0.349
F 35	8.2 - 10.5	0.74 - 0.95	1.718	1.59	24 23,621	0.388
F 36	7.9 - 10.3	0.71 - 0.92	1.718	1.59	24 23,621	(0.388)**
G 25	5.9	0.53	1.718	1.59	- null -	0.258
G 37	9.0	0.81	1.718	1.59	- null -	0.383
G 39	8.8	0.79	1.718	1.59	- null -	0.372

* Time-averaged vertical stratification evaluated at 1/6 gap width from the cold wall between heights $z = (3/4)H$ and $z = (1/2)H$.

** estimated value

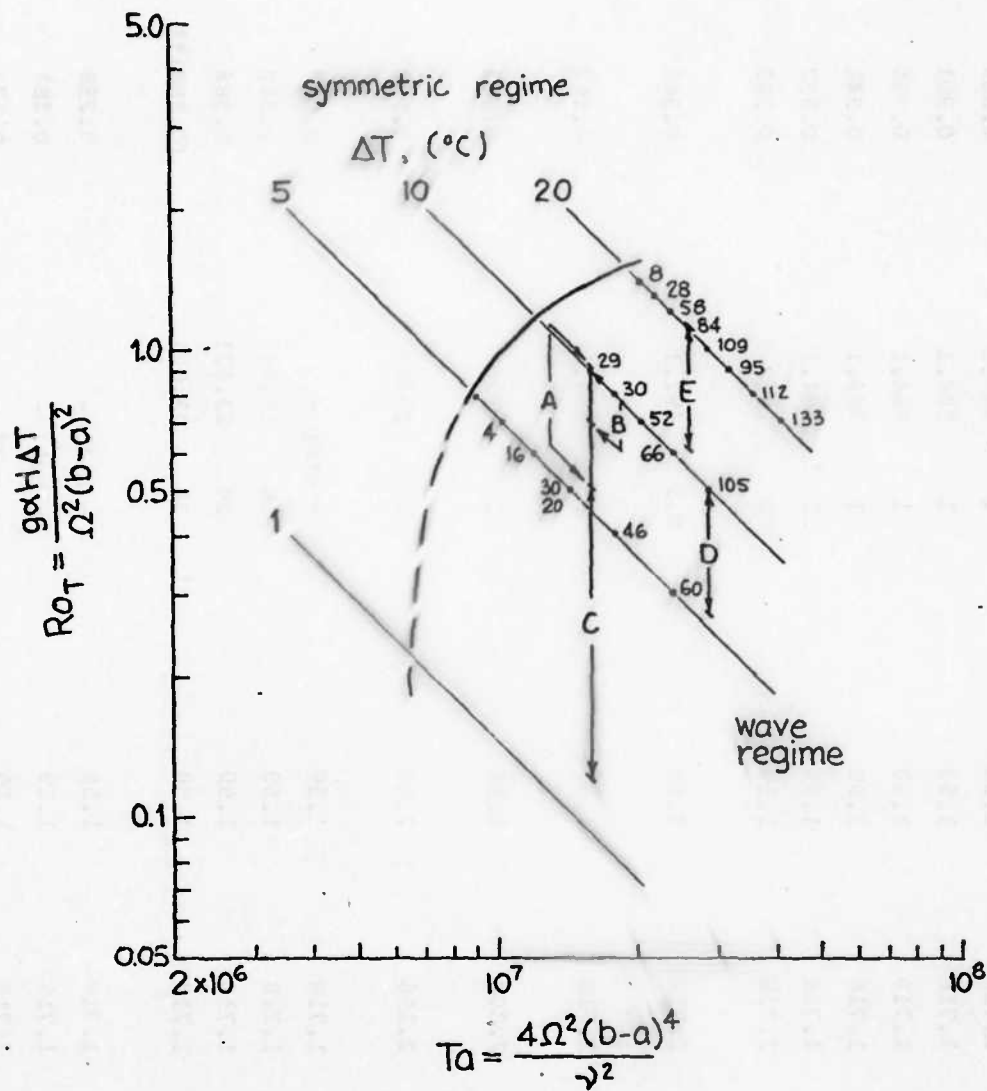


Fig. 3: Time-mean eddy thermal variances (V_E) corresponding to the experiments denoted by dots in fig. 2. The variances here have been converted to energy units (10^{-2} ergs cm^{-2}) by multiplying by the coefficient used in defining the available potential energy of a liquid.

with sufficient time allowed after each step-change for the fluid flow to reach a non-transient state with respect to the imposed external conditions. The purpose of these experiments was to elucidate the hysteresis characteristics of the system. Hysteresis was also studied by means of experiment SE-36, series F, in which T_i was varied continuously over a 24-hour period. This variation was sufficiently slow to permit the flow to keep up with the resulting changes in ΔT without displaying significant transient effects.

Experiments designated by the letters A, B, C, D and E in Table 1 and Fig. 2 were conducted with the rotation rate held fixed and with more rapid cyclic variations of the imposed temperature difference produced by continuously varying the temperature of the cold inner bath. In these experiments several different fixed rotation rates, and several different frequencies and amplitudes of the imposed temperature difference were employed.

5. Characteristic time scales

In order to facilitate the interpretation and understanding of the experimental results, we consider here several different characteristic time scales. These are (a) the amplitude vacillation periods, (b) the periods over which the imposed temperature contrast was varied, (c) the response times of the fluid (i.e., the e-folding times required for the fluid to respond to step changes in T_i), and (d) the lag times required for the fluid to

respond to cyclic variations in T_i .

(a) The amplitude vacillation periods: The characteristics of amplitude vacillation were described by Pfeffer, Buzyna and Fowlis (1974). The vacillation period is an internal scale resulting from the general dynamics of the flow. For given externally-imposed parameters (either fixed or transient) the vacillation periods of successively higher wave numbers in these experiments were successively shorter (see Table 2). This was the case when different wave numbers coexisted in the same experiment, and when the dominant wave number changed during an experiment. It was also the case when different wave numbers formed as a consequence of repeating an experiment at the same point in dimensionless-parameter space. For example, in experiment SE-29 (series A) the dominant modes occurring at different times with different relative magnitudes were wave numbers 3, 4, and 5. Their characteristic vacillation periods were approximately 130, 60, and 53 rot, respectively. The vacillation period of each mode was also observed to decrease with successively higher rotation rates. For example, at the higher rotation rate of experiment SE-30 (series E), the dominant modes were again wave numbers 3, 4, and 5. The vacillation periods of these modes in this experiment were approximately 120, 50, and 44 rot, respectively. The greatest uncertainty in these determinations is in the vacillation period of wave number 3 because this mode occurs with sufficiently large amplitude only over one or two major amplitude vacillation cycles. Hence, the vacillation periods

TABLE 2

Group	Experiment No.	Cycle Period (rotations)	Vacillation Period (Rotations)				
			Wave #3	Wave #4	Wave#5		
A	SE-26	984.1	-	62	52		
A	SE-29	1968	~130	60	53		
B	SE-31	492.1	-	63	56		
E	SE-30	2516	~120	50	44		

reported for this wave number should be regarded only as crude estimates.

(b) The periods of the imposed temperature contrast:

These periods were deliberately set to be long in comparison with the thermal lag time of the fluid and with the vacillation periods observed in null experiments. The imposed periods employed were 1/2, 1, 2, 16, and 24 hours. The 16- and 24-hour periods were selected for the purpose of studying hysteresis. The 1/2 to 2 hour imposed cycles represent periods ranging from 492 to 2516 rot, depending upon the rotation rate in each experiment (see Table 2). In most experiments these periods were more than ten times longer than the vacillation period and from six to nine times longer than the thermal lag times of the fluid. The shortest imposed temperature contrast period (experiment SE-31) was 7.8 times as long as the observed vacillation period in that experiment and 3 times longer than the thermal lag time.

(c) The thermal response times: The response times of the zonally averaged temperature (\bar{T}) at different radii and depths to a step-change in external conditions depend upon the physical properties of the system (e.g., mass, thermal diffusivity), the efficiency of the eddy and symmetric convection and the position relative to the boundaries. In our experiments the response times to a step-change in T_i were observed to increase, and the magnitude of the changes in \bar{T} to decrease, with distance from the cold inner wall. For example, in experiment SE-32 (series F) the e-folding response times at mid-depth at 1/6, 1/2, and 5/6

gap-widths measured from the inner wall were approximately 1140, 1310, and 1600 sec (312, 358, and 437 rot), respectively. The changes in \bar{T} at these radii were approximately 1.8, 1.6, and 1.4°C, respectively. Moreover, since the 'step' change in T_i was actually accomplished at the thermal controls of the circulating bath, T_i also exhibited a response time. In experiment SE-32 this time was measured to be 315 sec (86 rot), which should be subtracted from the response times in the fluid interior in order to measure the effect of the fluid convection.

(d) The lag times: The mean lag times and amplitudes of the \bar{T} variations at different locations in the annulus in response to cyclic variations of T_i depend upon the same factors as do the thermal response times and amplitudes following step-changes in T_i . In addition, they depend upon the frequency of the imposed cyclic variation. In our experiments the mean lag times were observed to increase, and the amplitudes of the \bar{T} variations to decrease, with distance from the inner wall. With progressively longer periods of the imposed cyclic variation the amplitudes of the internal temperature variations were progressively larger, and the lag times, although longer in absolute time, represented a progressively smaller fraction of the imposed cycle. These properties may be illustrated in the case of experiments SE-05 and SE-29 (series-A) in which T_i was cycled with periods of 984.1 and 1968 rot, respectively, between temperature extremes which were not too different from each other. The amplitudes of the \bar{T} variations at mid-depth at various radii in the annulus

were, on average, smaller by 50% and 20%, respectively, than the difference in amplitude between the temperatures at the same locations in null experiments corresponding to the two extremes of the imposed cycle. The lag times in these experiments are given in Table 3.

6. Low pass filtering of the data

Our interest in the present study is primarily in the responses of the fluid system to imposed variations of T_i . As indicated in Table 2, the periods of the imposed temperature variation are considerably greater than the periods of amplitude vacillation. In order to bring out more clearly the longer-period responses to the imposed temperature variation, we used a low-pass filter to suppress the relatively shorter-period amplitude vacillation. The filter was constructed in the following manner: The original data obtained at any one location consists of one temperature measurement every four, five, or six rot depending upon the rotation rate of the experiment. A moving average of 21 consecutive temperature measurements was performed first, with each point given equal weight. The resulting averages were then subjected to a second 21-point moving average. These averages were, in turn, subjected to a third 21-point moving average to complete the construction of the filter. Each of the smoothed temperature values in the resulting time sequence contains contributions from temperatures measured at 61 different times weighted as shown in Fig. 4. This figure also shows the

TABLE 3

Lag times at mid-depth at three radii in percent of cycle period

Experiment	Radius (gap width)		
	1/6	1/2	5/6
SE-05	16%	18%	20%
SE-29	10%	11%	12%

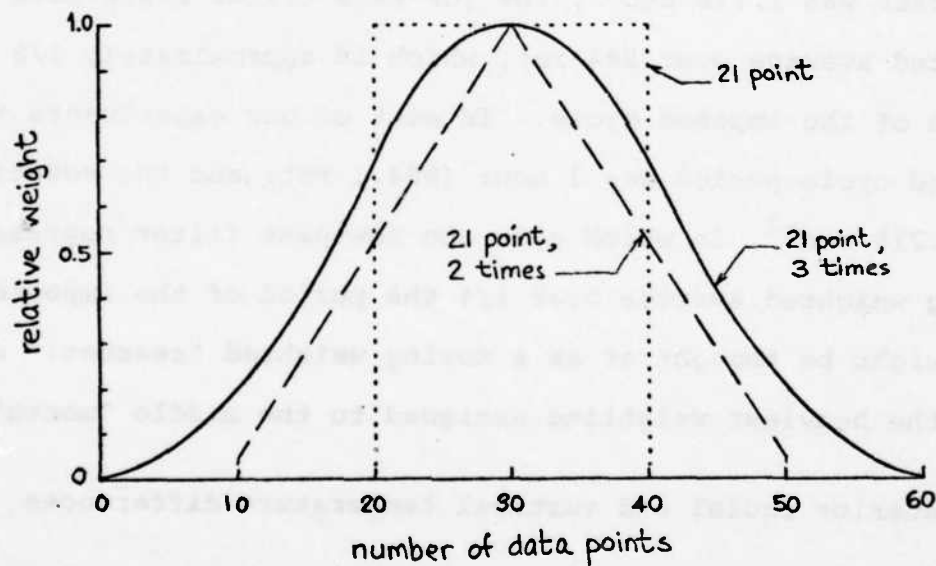


Fig. 4 Distribution of relative weights used in smoothing the data. Distributions are shown for three successive passes of the 21-point moving average, in which each point is given equal relative weight.

effect of each pass of the 21-point moving average on the relative weights assigned to each temperature in the time sequence.

The effect of smoothing the data of experiment SE-29 (series A) is shown in Figs. 5a, and 5b. Fig. 5a shows the time variation of both the smoothed and unsmoothed square of the amplitude of wave number 4 for two externally imposed cycles. Fig. 5b shows a similar comparison for the eddy thermal variance over the same two cycles. The imposed variation of T_i is depicted by the dotted curve. In this experiment, in which the imposed cycle period was 2 hours (1968 rot), and the basic rotation rate was 1.718 sec^{-1} , the low-pass filter represents a weighted average over 244 rot, which is approximately $1/8$ the period of the imposed cycle. In most of our experiments the imposed cycle period was 1 hour (984.1 rot) and the rotation rate was 1.718 sec^{-1} , in which case the low-pass filter represents a moving weighted average over $1/4$ the period of the imposed cycle. This might be thought of as a moving weighted "seasonal" average with the heaviest weighting assigned to the middle "month".

7. Interior radial and vertical temperature differences

The low-pass filter was applied also to the data obtained from experiments in which the thermostat controlling T_i was changed in steps. The responses of the filtered \bar{T} 's at mid-depth, at $1/6$, $1/2$, and $5/6$ gap-widths measured from the inner wall, following a near-step-change in T_i from 24.4 to 19.7°C in experiment SE-32 (series F), are shown in Fig. 6. Also shown is the

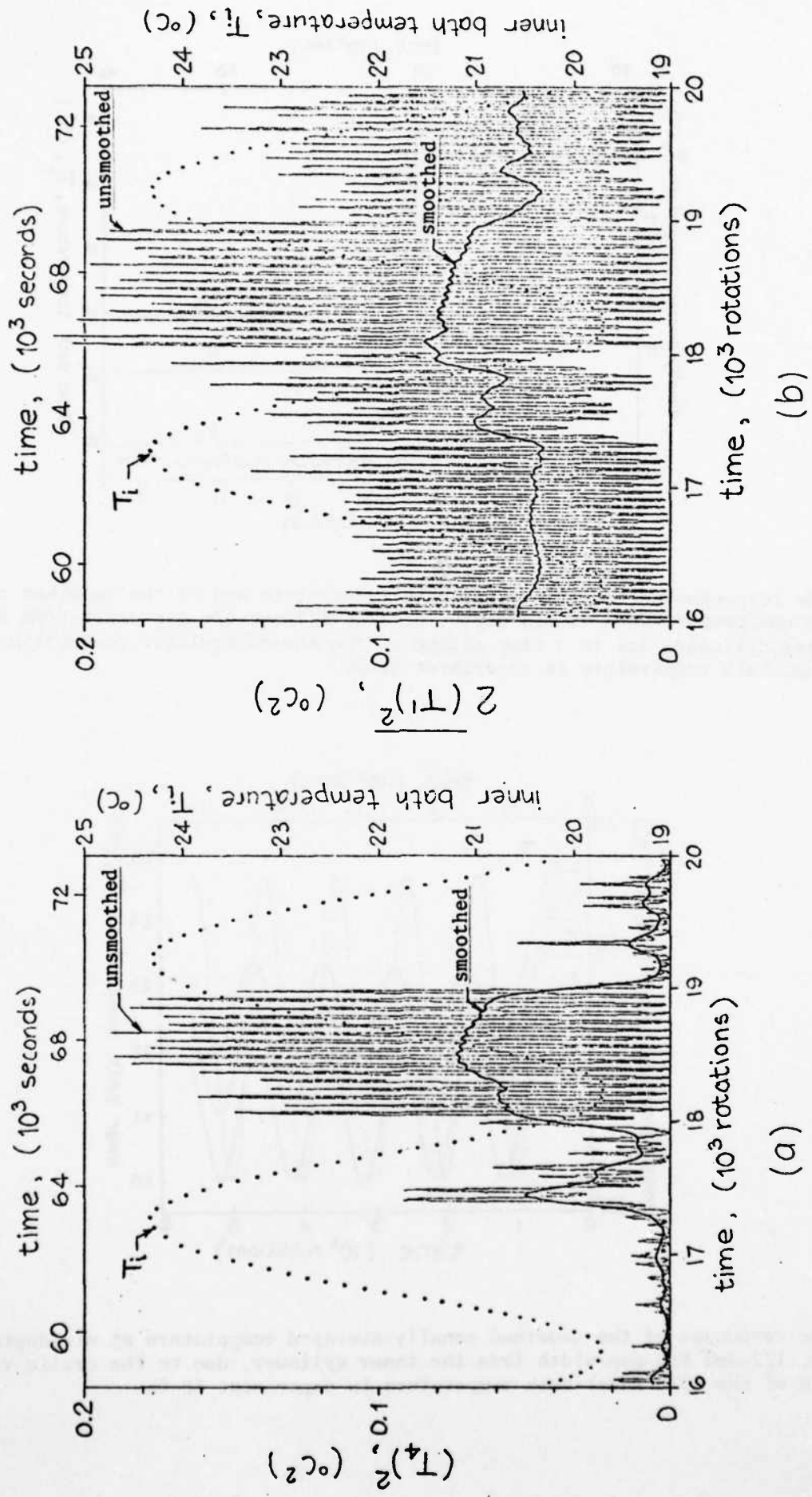


Fig. 5: A time-segment of data from mid-depth and mid-gap-width in experiment SE-29 showing both unsmoothed and smoothed records obtained by applying three successive passes of the 21-point moving average. (a) Thermal variance of wave number 4, $(T_4)^2$. (b) Eddy thermal variance, $(T_1)^2$.

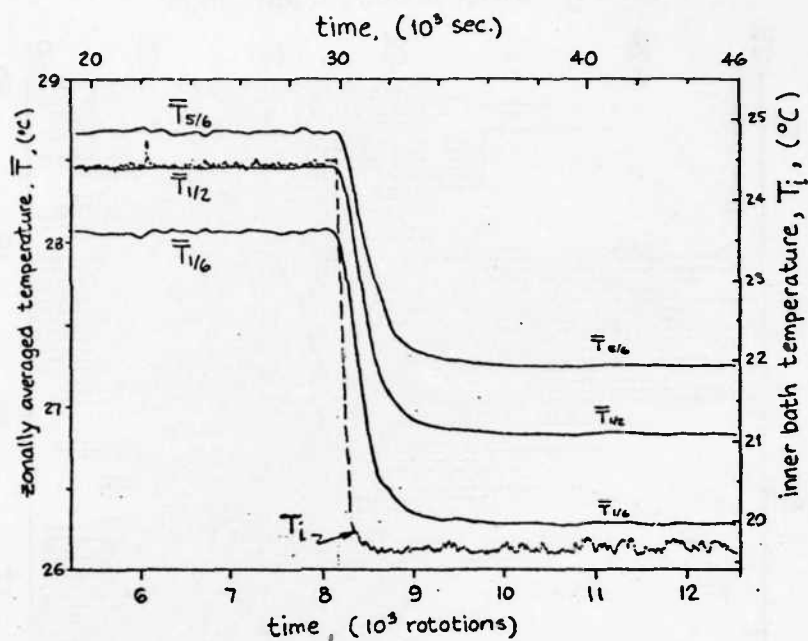


Fig. 6: Time responses of the inner cold-bath temperature and of the smoothed zonally-averaged temperatures at mid-depth, at 1/6, 1/2 and 5/6 gap-width from the inner cylinder, due to a step change of the thermoregulator controlling the inner-bath temperature in experiment SE-32.

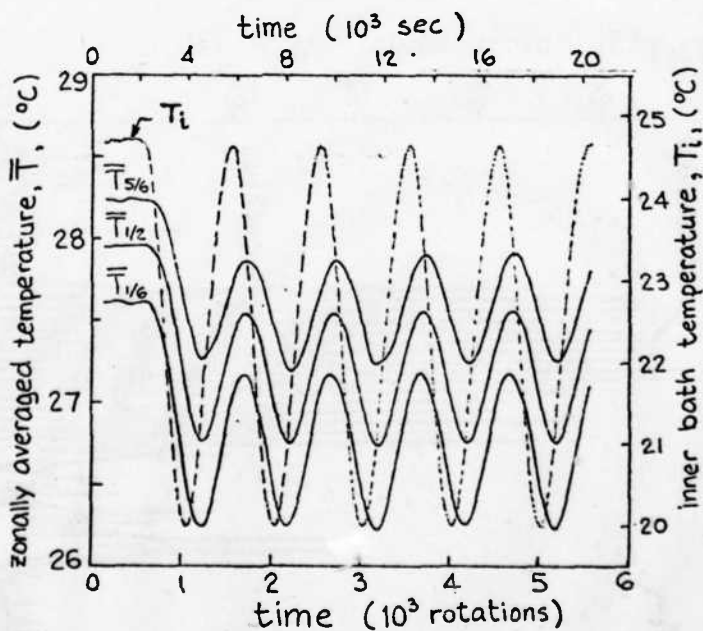


Fig. 7: Time responses of the smoothed zonally-averaged temperature at mid-depth, at 1/6, 1/2 and 5/6 gap-width from the inner cylinder, due to the cyclic variation of the cold inner-bath temperature in experiment SE-05

response of T_i to the change in the thermostat. The scale for T_i appears on the right hand side of the diagram. The inner-bath temperature and the filtered temperatures in the interior of the working fluid appear to have exponential responses. These are the curves which provided the data for the e-folding times reported earlier.

Fig. 7 shows the response of the filtered \bar{T} 's at mid-depth, at 1/6, 1/2, and 5/6 gap-widths, to cyclic variations of T_i between 20.0 and 24.7°C in experiment SE-05 (series A). The scale for T_i appears on the right. These curves provided the data for the lag times reported earlier.

From the data in Figs. 6 and 7 we may calculate the response of the filtered temperature difference $(\bar{T}_{5/6} - \bar{T}_{1/6})$, which serves as a crude measure of the zonally-averaged temperature gradient in the vicinity of mid-radius. Since the zonally-averaged temperatures at 5/6 and 1/6 gap-width have different response times to a step change in T_i , due to their different positions relative to the forcing boundary, the response curve for the difference between these two temperatures is not a simple decaying exponential. To illustrate this point we may consider an idealized model of exponentially decaying temperature responses at the two radii

$$\bar{T}_{1/6} = a + be^{-t/c} \quad (1)$$

$$\bar{T}_{5/6} = d + ge^{-t/h} \quad (2)$$

whereby it follows that

$$\bar{T}_{5/6} - \bar{T}_{1/6} = f + ge^{-t/h} - be^{-t/c} \quad (f \equiv d - a) \quad (3)$$

The solid curve in Fig. 8a shows the idealized response curve for the difference $(\bar{T}_{5/6} - \bar{T}_{1/6})$ using the values $a = 26.28^\circ\text{C}$, $b = 1.80^\circ\text{C}$, $c = 1140$ sec, $d = 27.22^\circ\text{C}$, $g = 1.44^\circ\text{C}$ and $h = 1600$ sec, corresponding to experiment SE-32 (Fig. 6). The most notable feature of this curve is the considerable overshoot around 2000 sec. This curve may be compared with the dashed curve which shows the response which would occur if the exponential decay rate of $\bar{T}_{5/6}$ were equal to that of $\bar{T}_{1/6}$ (i.e., if $h = c = 1140$ sec). The actual response of the difference $(\bar{T}_{5/6} - \bar{T}_{1/6})$ in experiment SE-32, shown in Fig. 8b, displays a steeper and larger overshoot which, as shown later in Fig. 13, is accompanied by a wave number change at the time of the peak. Figure 9 shows the observed response of the filtered temperature difference $(\bar{T}_{5/6} - \bar{T}_{1/6})$ to wave number transition at effectively constant imposed temperature contrast during a section of experiment SE-34 (series F). The notable feature here is the peak in the temperature difference at the time of the wave number change.

We consider now the lag time of the smoothed temperature difference $\bar{T}_{5/6} - \bar{T}_{1/6}$ due to a cyclic variation of T_i . The temperature variations at the two radii may be expressed in the form

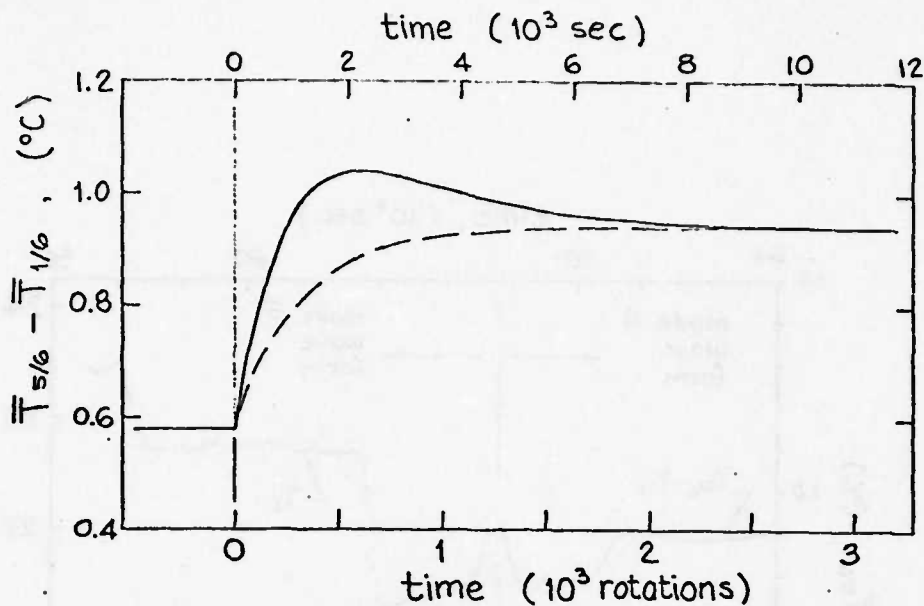


Fig. 8a: Theoretical response of the smoothed zonally-averaged temperature difference ($\bar{T}_{5/6} - \bar{T}_{1/6}$) to a step-change in the cold bath temperature obtained from equation (5). The solid curve is determined using coefficients corresponding to the smoothed mid-depth data of experiment SE-32. The dashed curve is obtained using the same values of f , g , b and c , but setting $h=c=1140$ sec corresponding to a hypothetical case in which the exponential decay rate of $\bar{T}_{5/6}$ is equal to that of $\bar{T}_{1/6}$.

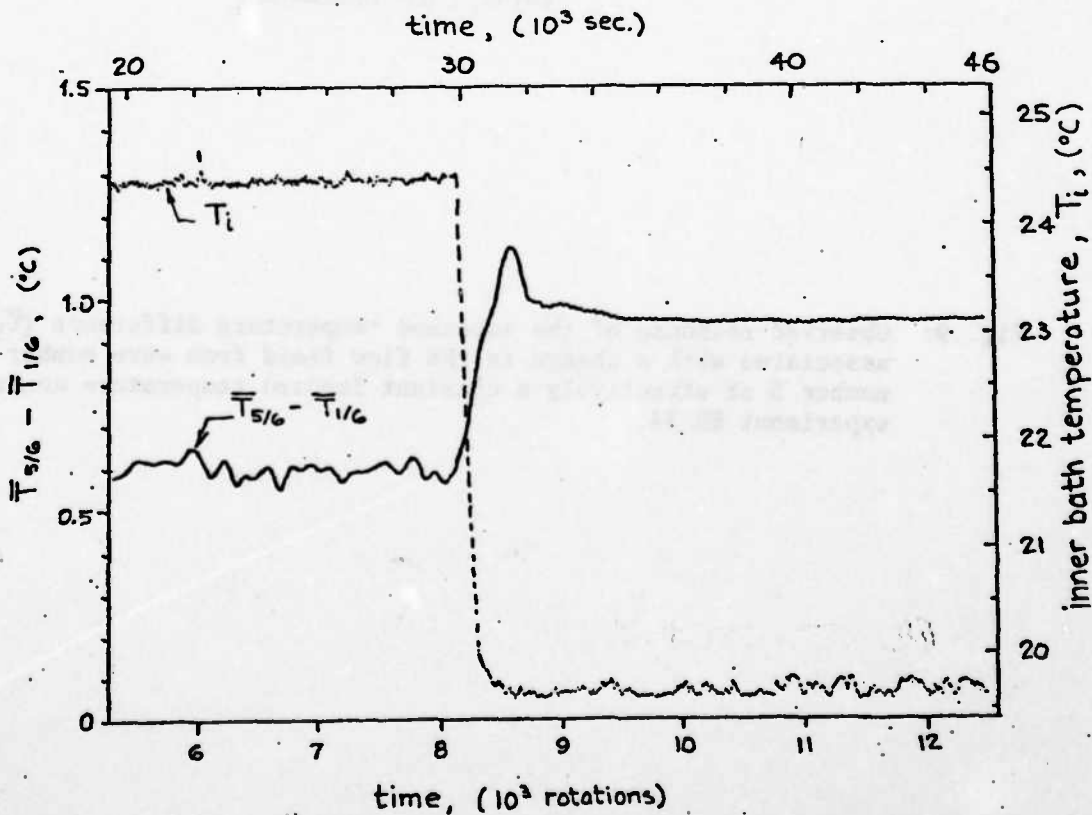


Fig. 8b: Observed response of ($\bar{T}_{5/6} - \bar{T}_{1/6}$) at mid-depth in the fluid to a near step-change in the cold inner-bath temperature in experiment SE-32.

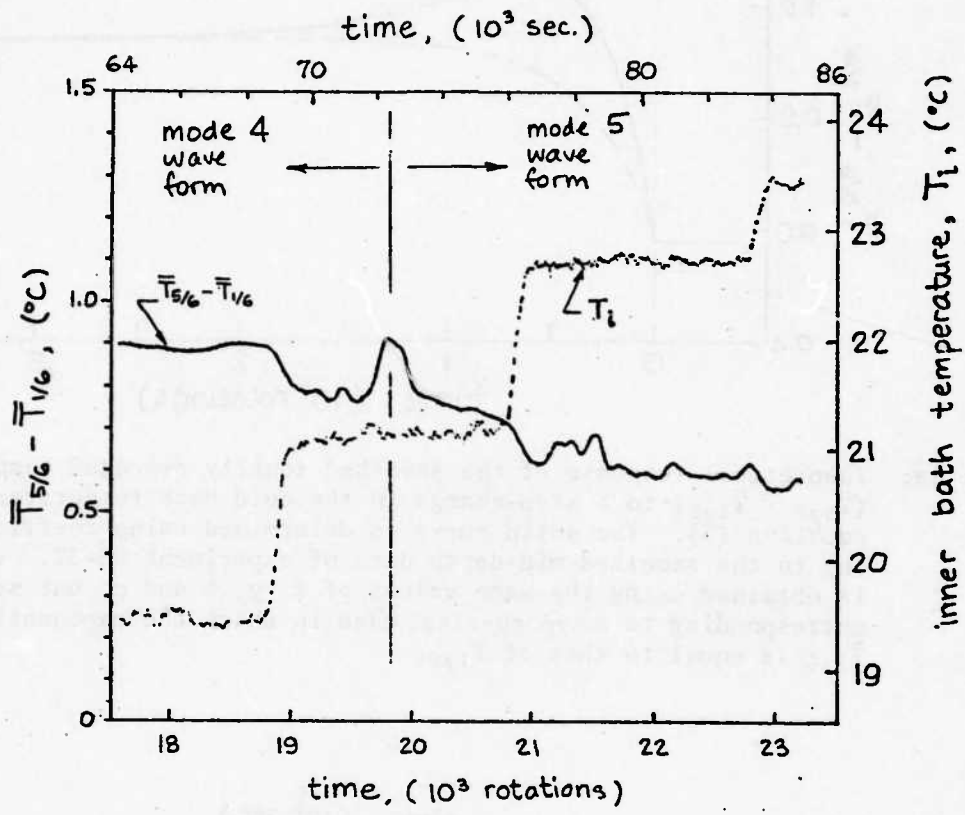


Fig. 9: Observed response of the smoothed temperature difference ($\bar{T}_{5/6} - \bar{T}_{1/6}$) associated with a change in the flow field from wave number 4 to wave number 5 at effectively a constant imposed temperature contrast during experiment SE-34.

$$\bar{T}_{1/6} = m + n \sin (\sigma t - \epsilon) \quad (4)$$

$$\bar{T}_{5/6} = p + q \sin (\sigma t - \eta) \quad (5)$$

where σ is the frequency of the oscillation and ϵ and η are the time lags between the cold bath temperature variation and the variations of $\bar{T}_{1/6}$ and $\bar{T}_{5/6}$, respectively. It follows that

$$\begin{aligned} \bar{T}_{5/6} - \bar{T}_{1/6} &= r + q \sin (\sigma t - \eta) - n \sin (\sigma t - \epsilon), \\ (r &\equiv p - m) \end{aligned} \quad (6)$$

or,

$$\bar{T}_{5/6} - \bar{T}_{1/6} = r + D \sin (\sigma t - \alpha) \quad (7)$$

where $D = \pm \sqrt{(q^2 + n^2) - 2nq \cos (\eta - \epsilon)}$, $\alpha = \tan^{-1} \left(\frac{q \sin \eta - n \sin \epsilon}{q \cos \eta - n \cos \epsilon} \right)$

and the sign of D is chosen such as to make the preceding two expressions mutually consistent. The solid curve in Fig. 10a shows the idealized response curve for the difference $(\bar{T}_{5/6} - \bar{T}_{1/6})$ using the values $m = 26.71^\circ\text{C}$, $n = 0.47^\circ\text{C}$, $p = 27.56^\circ\text{C}$, $q = 0.33^\circ\text{C}$, $\epsilon = 56$ deg and $\eta = 71$ deg corresponding to experiment SE-05 (Fig. 7). The dashed curve shows the response which would result if $\eta = \epsilon = 56$ deg. The notable feature here is the larger amplitude and earlier response of the solid curve to the imposed variation of T_i (dotted curve). The actual response of the smoothed

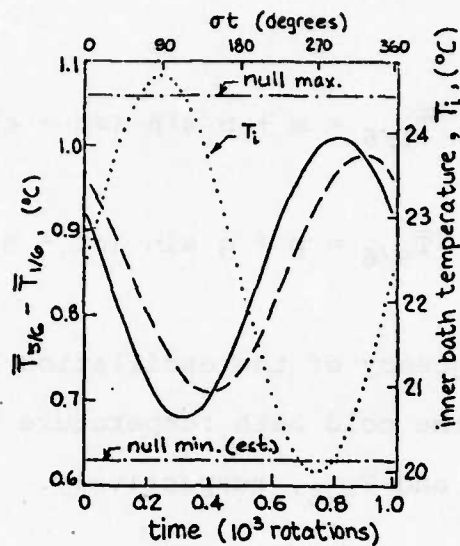


Fig. 10a: Theoretical response of the smoothed zonally-averaged temperature difference ($\bar{T}_{5/6} - \bar{T}_{1/6}$) to a cyclic variation of the cold inner-bath temperature obtained from equation 7. The solid curve was determined using coefficients associated with the smoothed mid-depth data of experiment SE-05. The dashed curve is obtained using the same values of m , n , p , q and ϵ , but setting $\eta = \epsilon = 56^\circ$ corresponding to a hypothetical case in which the lag of $\bar{T}_{5/6}$ is the same as $\bar{T}_{1/6}$, but the amplitude of $\bar{T}_{5/6}$ is smaller than that of $\bar{T}_{1/6}$. The dash-dot-dotted lines represent the estimated maximum and minimum values of the temperature difference ($\bar{T}_{5/6} - \bar{T}_{1/6}$) corresponding to the maximum and minimum imposed temperature contrast, respectively, in the absence of cyclic variation of the cold inner-bath temperature.

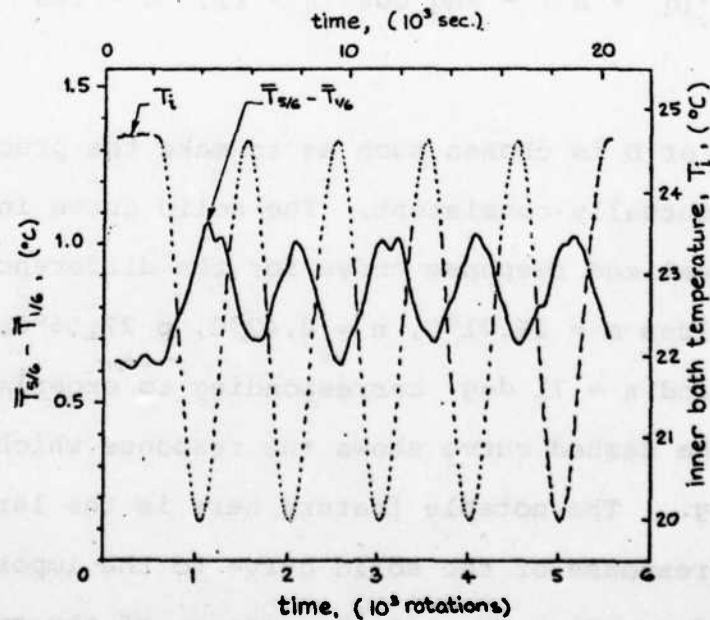


Fig. 10b: Observed response of the smoothed zonally-averaged temperature difference ($\bar{T}_{5/6} - \bar{T}_{1/6}$) at mid-depth in the fluid to the cyclic variation of the cold inner-bath temperature in experiment SE-05.

temperature difference ($\bar{T}_{5/6} - \bar{T}_{1/6}$) to the imposed cyclic variation of the cold bath temperature in experiment SE-05 is shown in Fig. 10b. The average lag between the minimum T_i (i.e., maximum imposed ΔT) and the maximum internal temperature difference ($\bar{T}_{5/6} - \bar{T}_{1/6}$) is 30 ± 9 deg vs the predicted value of $\alpha = 26.5$ deg shown in Fig. 10a.

Finally, we present the response of the smoothed vertical temperature difference in the interior of the fluid to the imposed cyclic variation of T_i in experiment SE-05. The network of thermistors used in this study enabled us to estimate the vertical stratification only at $1/6$ gap-width from the cold wall and only in the layer $1/2 H < z < 3/4 H$. The time variation of the temperature difference between these two levels at $1/6$ gap-width is shown by the solid curve in Fig. 11. The stratifications at larger radii can be expected to display greater time lags with respect to the cyclic variation of T_i (dashed curve).

8. Null experiments

Null experiments are defined here as experiments in which the externally controlled parameters (rotation rate and imposed temperature contrast) are held fixed. These are conventional annulus experiments. In this section we shall discuss pertinent results of previously unpublished ^{null} experiments performed with a two-level network of 100 thermistors, as well as results of three additional null experiments conducted in order to supplement our knowledge of the time-dependent behavior of the fluid at

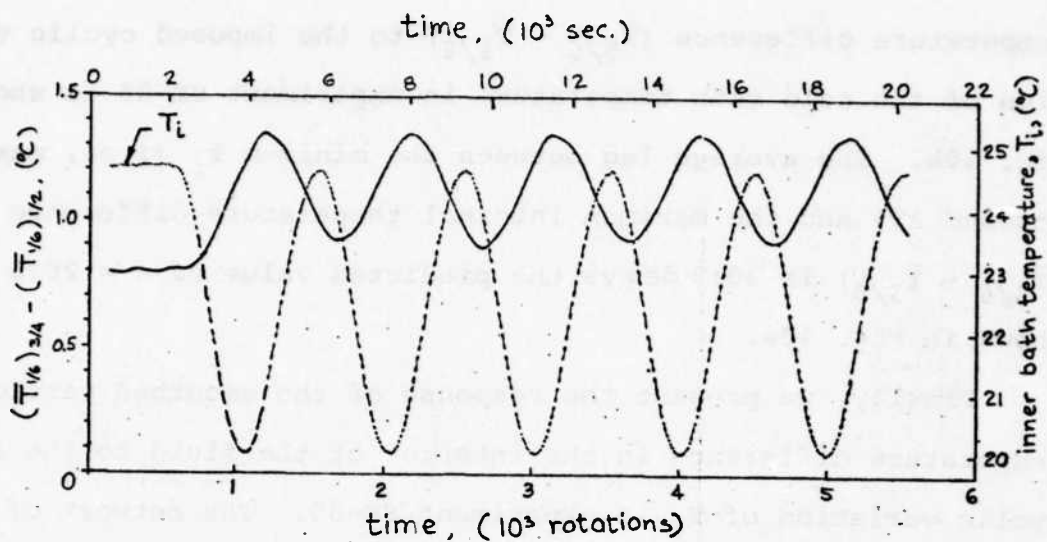


Fig. 11: Observed response of the smoothed vertical temperature difference at 1/6 gap-width from the inner cylinder in experiment SE-05. The vertical temperature difference $[(\bar{T}_{1/6})_{3/4} - (\bar{T}_{1/6})_{1/2}]$ was obtained from the zonally-averaged temperatures at heights $z = 3/4 H$ and $z = 1/2 H$.

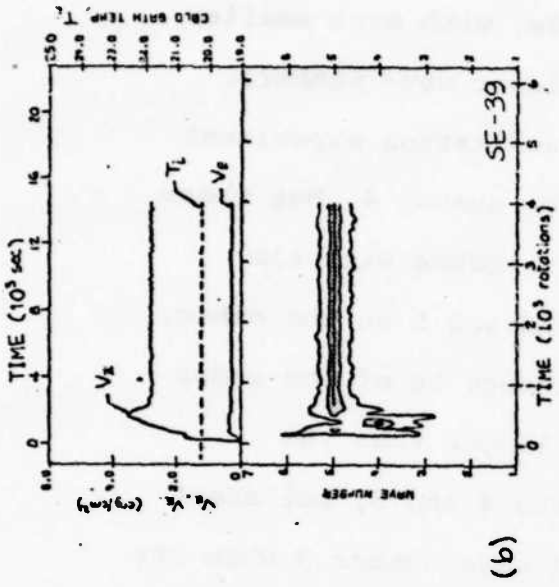
significant points in dimensionless-parameter space. Such information provides a useful framework within which to interpret the results of experiments with imposed cyclic variations of T_i .

(The three new experiments are listed in Table 1 as series G and are designated in Fig. 2 by crosses.) In addition, we shall present the results of experiment SE-32, in which the imposed ΔT was changed abruptly from 5.9 to 10.6°C by changing T_i from 24.4 to 19.7°C.

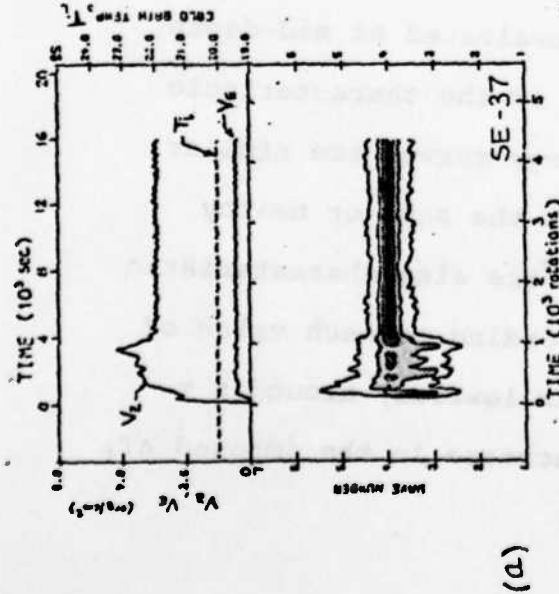
In all null experiments presented here the annulus was maintained stationary at first while the hot and cold temperature baths were brought to the required equilibrium values. The rotation rate of the turntable was then set to the specified value. After initial spin up, the flow normally exhibited further transient characteristics before settling down to a statistically identifiable behavior which we define as the characteristic behavior at the particular point in dimensionless-parameter space.

Figs. 12a, b, and c present contours of the *filtered* eddy temperature variance at mid-depth and mid-gap-width as a function of wave number and time in experiments SE-37, 39, and 25, respectively. Contours are used here for convenience although it is recognized that the variance spectra are discrete. Above each figure is a plot of the time variations of the filtered zonal and eddy temperature variances (V_z and V_E , respectively) evaluated at mid-depth, and of the imposed cold bath temperatures. Experiments SE-37, 39, and 25 are characterized by 4-wave

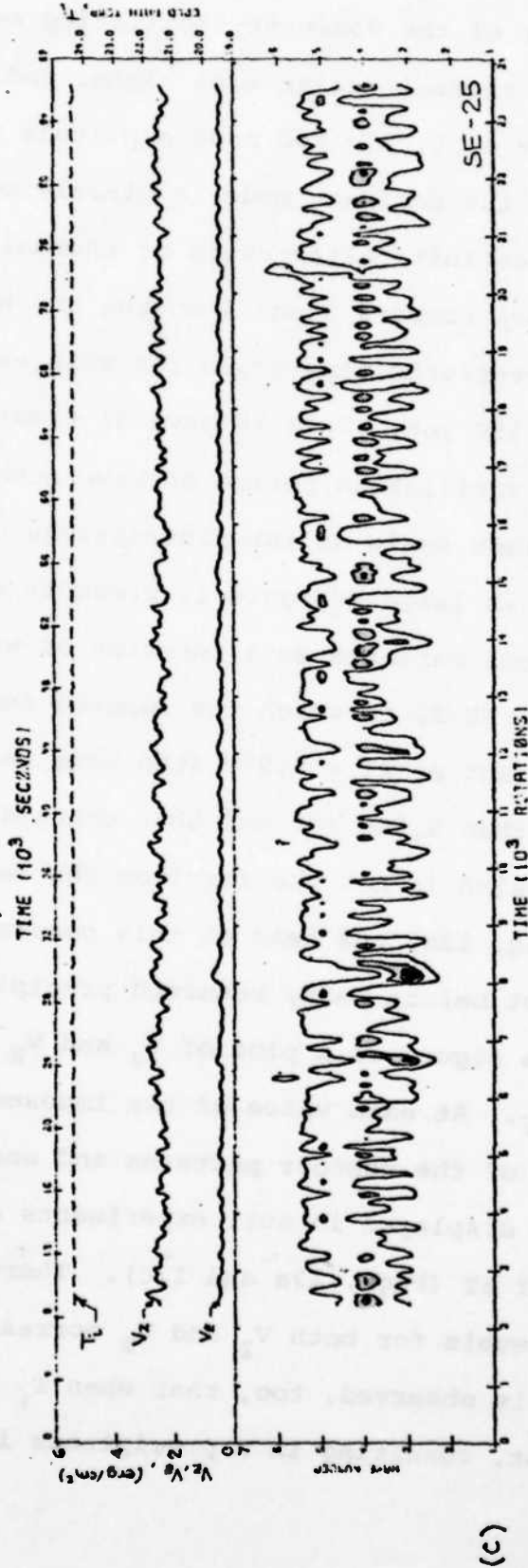
amplitude vacillation, 5-wave amplitude vacillation and 4, 5, 3 mixed mode amplitude vacillation, respectively. In the 4- and 5-wave amplitude vacillation cases data were taken starting prior to experimental time zero (i.e., the time at which the rotation rate was suddenly changed from zero to the specified value). Accordingly, Figs. 12a and b show clearly the transient states in these two experiments. In both cases the transient states are characterized by a broader variance spectrum and a larger zonal temperature variance than in the remaining portion of each experiment. It is interesting to note, however, that although these two experiments are very close to each other in dimensionless-parameter space ($Ro_T = 0.81$ and $Ro_T = 0.79$, respectively), the transient is shorter in duration in the 5-wave amplitude vacillation experiment than it is in the 4-wave vacillation experiment. Another interesting feature is the sharp peak in V_z in both cases just prior to the formation of the long-term non-transient pattern. We believe this is due to the inefficiency of the broader spectrum of waves present during the transient stage in transporting heat "poleward", thus leading to a continued rise in V_z until the preferred mode becomes well established and begins to transport sufficient amounts of heat "poleward" to balance the rate of generation of V_z by differential heating. As noted earlier, amplitude vacillations are smoothed out of the data by the low pass filter. Accordingly, the non-transient portion of each record is characterized in Figs. 12a, b, and c by a steady thermal variance maximum at the



(b)



(d)



(c)

Figs. 12 a, b, c: The lower portions of these figures display contours of the smoothed temperature variance at mid-depth and mid-gap-width as a function of azimuthal wave number and time in the series G null experiments, SE-37 ($\Delta T = 9.0^\circ\text{C}$), SE-39 ($\Delta T = 8.8^\circ\text{C}$) and SE-25 ($\Delta T = 5.9^\circ\text{C}$). The rotation rate in each of these experiments was $\Omega = 1.718 \text{ sec}^{-1}$. Although the variance spectra are discrete, contours were used in these figures to aid in the visualization of the time sequences. Contour intervals are denoted by different shadings as follows: from 0.01 to 0.03°C^2 by \square ; from 0.03 to 0.05°C^2 by \square ; from 0.05 to 0.07°C^2 by \square ; and from 0.07 to 0.09°C^2 by \square . The upper portion of each figure shows the time variation of the cold inner-bath temperature (dashed curve) and of the zonal and eddy temperature variances V_z and V_e , respectively, at mid-depth (solid curves). Here, the variances have been converted to energy units (erg cm^{-2}) by multiplying by the coefficient used in defining the available potential energy of a liquid. The required static stability parameter in the denominator of this coefficient was obtained from the vertical temperature difference $[(T_1/6)^{3/4} - (T_1/6)^{1/2}]$ averaged over the length of the record excluding the transient portions of experiments SE-37 and SE-39. The time averaged values of the vertical stratification at $1/6$ gap-width used in these and all other experiments are given in Table 1.

wave number of the dominant vacillating mode, with much smaller amounts of thermal variance at higher and lower wave numbers.

In the 4, 5, 3 mixed mode amplitude vacillation experiment (Fig. 12c) the dominant mode is clearly wave number 4, but there is also a definite alternation of thermal variance with time between wave numbers 3 and 4 on the one hand and 5 on the other. The characteristic time-scale for this exchange is of the order of 125 to 150 rot. This is several times longer than the amplitude vacillation period of wave numbers 4 and 5, but about the same time scale as the fluctuations of wave number 3 when its amplitude is large. # Figure 13 presents contours of the filtered eddy thermal variance as a function of wave number and time in experiment SE-32 in which the imposed temperature contrast was held constant at $\Delta T = 5.9^\circ\text{C}$ (the same value as in SE-25, Fig. 12c) for more than 8,000 rot and then changed precipitously to $\Delta T = 10.6^\circ\text{C}$ (which is not too far from the value, $\Delta T = 9.0^\circ\text{C}$, in SE-37, Fig. 12a) and held at this constant value for more than 14,000 rot before being returned precipitously to $\Delta T = 5.9^\circ\text{C}$. Above the figure is a plot of V_z and V_E evaluated at mid-depth, and of T_i . At each value of the imposed ΔT the characteristic features of the contour patterns and energy curves are similar to those displayed in null experiments at the same or nearby values of ΔT (Figs. 12a and 12c). There are also characteristic energy levels for both V_z and V_E corresponding to each value of ΔT . It is observed, too, that when T_i is lowered, around $t = 8,150$ rot, resulting in a precipitous increase in the imposed ΔT ,

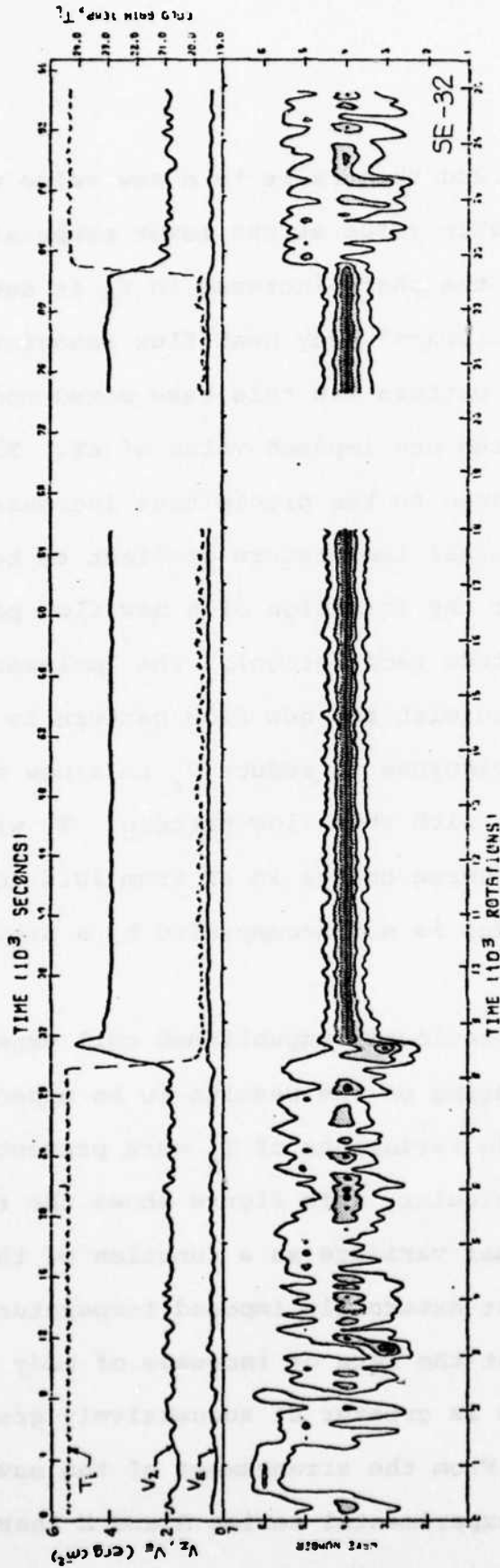


Fig. 13: Response of the temperature variance to near step-changes in the cold bath temperature of 4.6°C providing corresponding changes in the imposed temperature contrast between 5.9 and 10.5°C in experiment SE-32, series F. Quantities represented and contour values and intervals are the same as those in Fig. 12. The vertical stratification used in calculating the energy equivalent of V_z and V_v was determined from the time average of $[(\bar{T}_1/6)^{3/4} - (\bar{T}_1/6)^{1/2}]$ over the statistically-steady portions of the record excluding the transients between 8,000 and 9,000 rotations and between 22,000 and 23,000 rotations. The gap in the record is due to a temporary failure of the data acquisition system while the imposed conditions of the experiment continued uninterrupted.

V_z rises sharply to a peak and then falls to a new value which is larger than the characteristic value at the lower temperature contrast. We believe that the sharp increase in V_z is due mainly to the inefficiency of the "poleward" eddy heat flux associated with the pre-existing flow pattern (in this case mixed mode amplitude vacillation) at the new imposed value of ΔT . This enables V_z to rise in response to the precipitous increase in ΔT , and the associated internal temperature gradient to become baroclinically unstable for the formation of a new flow pattern (in this case 4-wave amplitude vacillation). The "poleward" eddy flux of heat associated with the new flow pattern is believed to be sufficiently vigorous to reduce V_z to a new characteristic level consistent with this flow pattern. It will be noted, however, that the reverse change in ΔT from 10.6 to 5.9°C (around $t = 22,570$ sec) is not accompanied by a similar overshoot.

Results derived from previously unpublished null experiments which have an important bearing on the results to be expected from experiments with cyclic variations of T_z were presented earlier in Fig. 3. In particular, this figure shows the relative magnitude of the eddy thermal variance as a function of the rotation rate at three different externally imposed temperature contrasts. Here we see that the rate of increase of eddy thermal variance with rotation rate is greater at successively greater values of the imposed ΔT . From the arrangement of the numbers, we can anticipate that in experimental series A and E there

should be little if any change in the eddy thermal variance from "summer" to "winter" as T_i is varied cyclically. Experiments C and D, on the other hand, would be expected to display greater eddy thermal variance in "winter" (i.e., at the higher values of the imposed temperature contrast) than in "summer", as does the earth's atmosphere.

Another feature of interest seen in Figs. 2 and 3 is that two different wave regimes (i.e., 5-wave amplitude vacillation and 6-wave amplitude vacillation) occurred when the experiment at $Ro_T = 0.50$ and $Ta = 1.43 \times 10^7$ was run on different days. The higher wave-number flow is seen to possess a lower level of eddy thermal variance. A similar result occurs in other experimental series at various points in dimensionless-parameter space.

9. Hysteresis experiments

Hysteresis experiments are ones in which one of the externally imposed parameters (e.g., ΔT or Ω) is varied extremely slowly from an initial to a final value and then back to the initial value. If hysteresis is present it manifests itself as a bi-modal response of the system to the forcing function such that different fluid behavior is observed at a given point in dimensionless-parameter space when it is traversed from different directions. Hysteresis in rotating annulus convection has been studied experimentally by Fultz, et al (1959) and Kaiser (1970), and theoretically by Cole (1971). This phenomenon has also been studied in terms of catastrophe theory by Lacher, McArthur and

Buzyna (1977). In this section we present some details of a hysteresis study conducted in the region of the regime diagram in which experimental series A was performed. The results provide background information which is useful for interpreting the data from experiments with cyclic variations of T_i .

Three hysteresis experiments were conducted (series F, experiments SE-34, 35, and 36). In experiment SE-34 the external temperature contrast was varied over a range of 4.5°C by varying the cold bath temperature in four steps over a period of 16 hours. Since the cold bath temperature at each step was maintained constant for 2 hours, the thermal response time of the fluid (which is about $1/5$ this length of time) is not an important factor for present considerations. Fig. 14 shows contours of the smoothed thermal variance as a function of wave number and time in this experiment. The step-like dashed curve above the contour diagram represents the time variation of T_i . The imposed temperature contrast, ΔT , indicated at each step, was changed from 10.6°C at the beginning of the experiment to 6.1°C , and then back to 10.6°C . The experiment was continued for another half cycle to $\Delta T = 5.8^\circ\text{C}$. The upper and lower solid curves above the contour diagram represent the time variations of the smoothed V_z and V_E , respectively, measured at mid-depth.

Fig. 14 reveals that hysteresis is indeed an important characteristic of the fluid behavior. The experiment begins with $\Delta T = 10.6^\circ\text{C}$, at which value wave number 4 is the dominant mode. (The amplitude vacillations of this and other modes

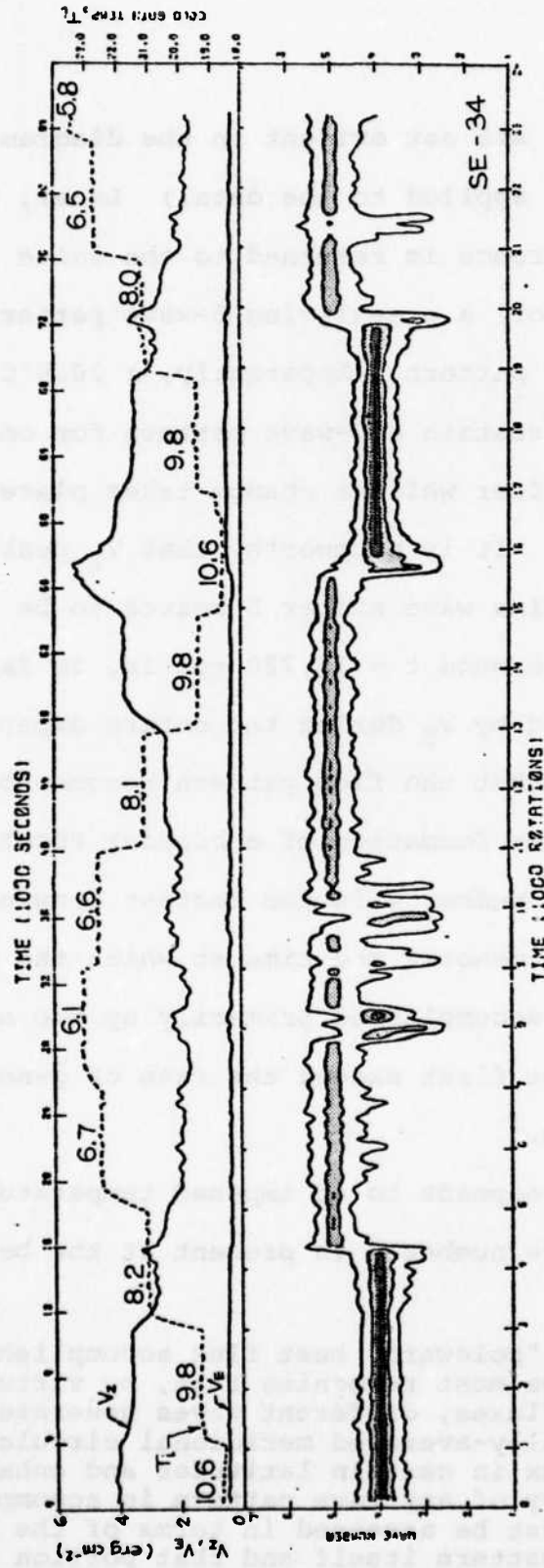


Fig. 14: Response of the temperature variance to small step-changes in the cold-bath temperature providing a range of corresponding imposed temperature contrasts from 5.8 to 10.6C in experiment SE-34, series F. Quantities represented and contour values and intervals are the same as in Figs 12 and 13. Numbers above each step of the cold bath temperature indicate the values of the imposed temperature contrast corresponding to that step. The vertical stratification used in calculating the energy equivalent of V_z and V_e is determined from the time average of $[(\bar{T}_{1/6})^{3/4} - (\bar{T}_{1/6})^{1/2}]$ over each of the steps in the first complete cycle.

throughout the experiment are not evident in the diagram because of the smoothing function applied to the data.) Later, when the imposed temperature difference is returned to the value $\Delta T = 10.6^\circ\text{C}$ ($15,000 < t < 16,890$ rot) a preexisting 5-wave pattern changes to a predominantly 4-wave pattern. Apparently, a 10.6°C imposed temperature contrast can sustain a 5-wave pattern for only a limited period of time, after which a change takes place to the preferred 4-wave pattern. It is noteworthy that V_z peaks in this interval, at which time wave number 5 ceases to be the dominant mode. The peak around $t = 15,720$ rot is, in fact, the largest magnitude attained by V_z during the entire experiment. At this point it appears that the flow pattern becomes baroclinically unstable for the formation of a broader spectrum of wave scales of which wave number 4 is the fastest growing mode. The peak in V_z apparently denotes the time at which the vigorous "poleward" heat flux accomplished primarily by the newly formed 4-wave pattern must first exceed the rate of generation of V_z by diabatic heating.³

The second step corresponds to an imposed temperature contrast of 9.8°C . When wave number 4 is present at the beginning

³In speaking of the "poleward" heat flux accomplished by one or more wave scales we must recognize that, by virtue of their heat and momentum fluxes, different waves generate different distributions of zonally-averaged meridional circulations which oppose the heat flux in certain latitudes and enhance it in others. The efficiency of any wave pattern in accomplishing a "poleward" heat flux must be assessed in terms of the net effect of both the wave pattern itself and that portion of the symmetric meridional circulation which it generates.

it remains during this step. However, when wave number 5 is already present, as it is when the condition $\Delta T = 9.8^\circ\text{C}$ is traversed from the opposite direction (during the time interval $13,090 \leq t \leq 14,870$ rot), the 5-wave configuration remains during the entire step. Thus, a 9.8°C imposed temperature contrast is capable of sustaining either a 4- or 5-wave amplitude vacillating pattern depending upon the initial conditions.

The third step corresponds to $\Delta T = 8.2^\circ\text{C}$. At this temperature contrast the preexisting 4-wave amplitude vacillation pattern can be sustained only for a comparatively short period of time before it changes to a predominantly 5-wave amplitude vacillation pattern. It is significant that there is a peak in V_z at the time the wave number changes, suggesting that the newly-formed 5-wave pattern at this point in dimensionless-parameter space is more efficient at transporting heat "poleward" than is the preexisting 4-wave pattern which permitted V_z to rise to this peak. Later, when the imposed temperature contrast $\Delta T = 8.1^\circ\text{C}$ is traversed from the opposite direction, during the time interval $11,320 \leq t \leq 12,850$ rot, the preexisting 5-wave pattern is sustained throughout the entire interval.

The fourth step corresponds to $\Delta T = 6.7^\circ\text{C}$. Here we see a tendency for spectrum broadening and a slight wavering of the preexisting 5-wave pattern. Later when $\Delta T = 6.6^\circ\text{C}$ is traversed from the opposite direction, a preexisting mixed mode amplitude vacillation changes to a wavering 5-wave amplitude vacillation. Finally, at $\Delta T = 6.1^\circ\text{C}$ the weakly wavering dominant 5-wave

configuration changes to a predominantly mixed mode vacillation which seems to be the preferred configuration at this value of the imposed temperature contrast. The final third of the figure displays essentially the same behavior under essentially the same imposed external conditions as the first third. In addition to the characteristics discussed thus far, it is also noteworthy that wave number changes are preceded and accompanied by spectral broadening. It may be recalled that this experiment was conducted in a region of the regime diagram (Fig. 3) in which the eddy thermal variance is no greater for $\Delta T = 10^\circ\text{C}$ than it is for $\Delta T = 5^\circ\text{C}$. Hence, the only observed changes in the magnitude of V_E (lower solid curve in the figure) are those associated with wave-number changes. In this connection, it is significant that the magnitude of V_E is measurably lower when wave number 5 is the dominant vacillating mode than when the flow is characterized by either a predominantly 4-wave or mixed-mode amplitude vacillation.

We turn now to Fig. 15 which displays the results of experiment SE-35. In this experiment the imposed temperature contrast was varied in smaller steps over the limited range $8.1 \leq \Delta T \leq 10.5^\circ\text{C}$ with Ω set at the same value as it was in experiment SE-34. In SE-35 the cold-bath temperature at each step was maintained constant for 3 hours. This experiment began with $\Delta T = 8.1^\circ\text{C}$, at which a dominant 5-wave amplitude vacillation developed and was sustained as long as the temperature contrast was maintained at this value. This behavior is consistent with that seen in Fig. 14.

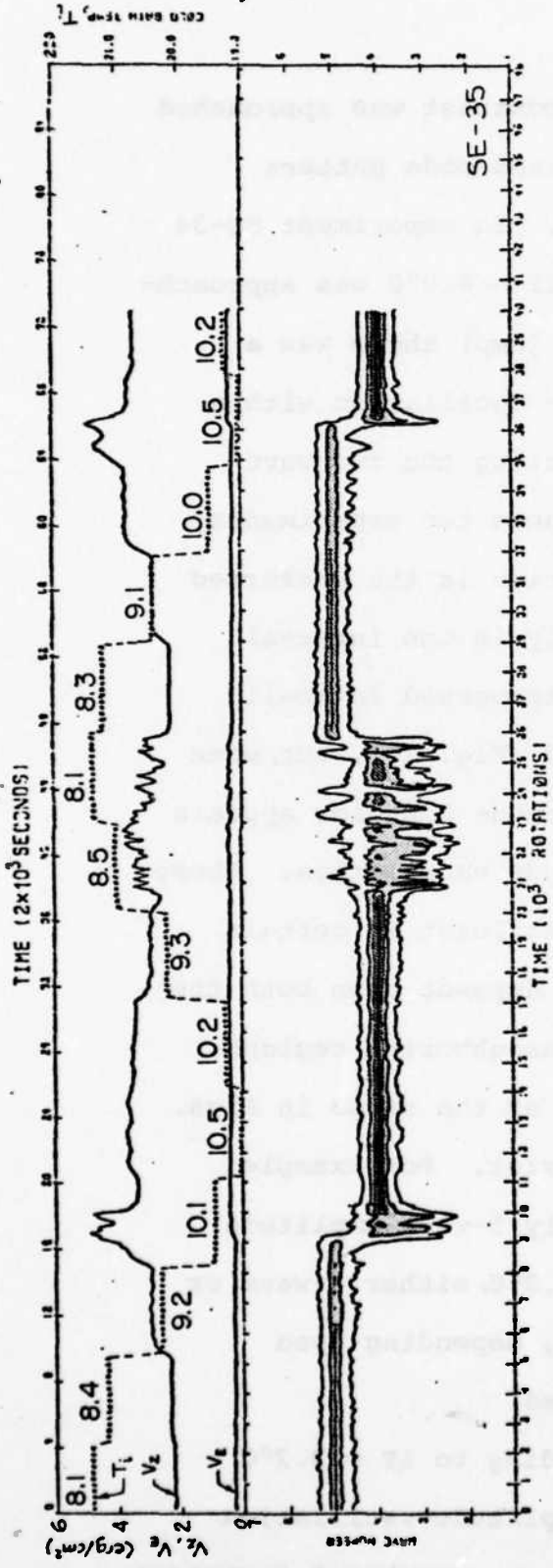


Fig. 15: Response of the temperature variance to small step-changes in the cold-bath temperature providing a range of corresponding imposed temperature contrasts from 8.1 to 10.5°C in experiment SE-35, series F. Quantities represented and remaining comments are the same as in Fig. 14.

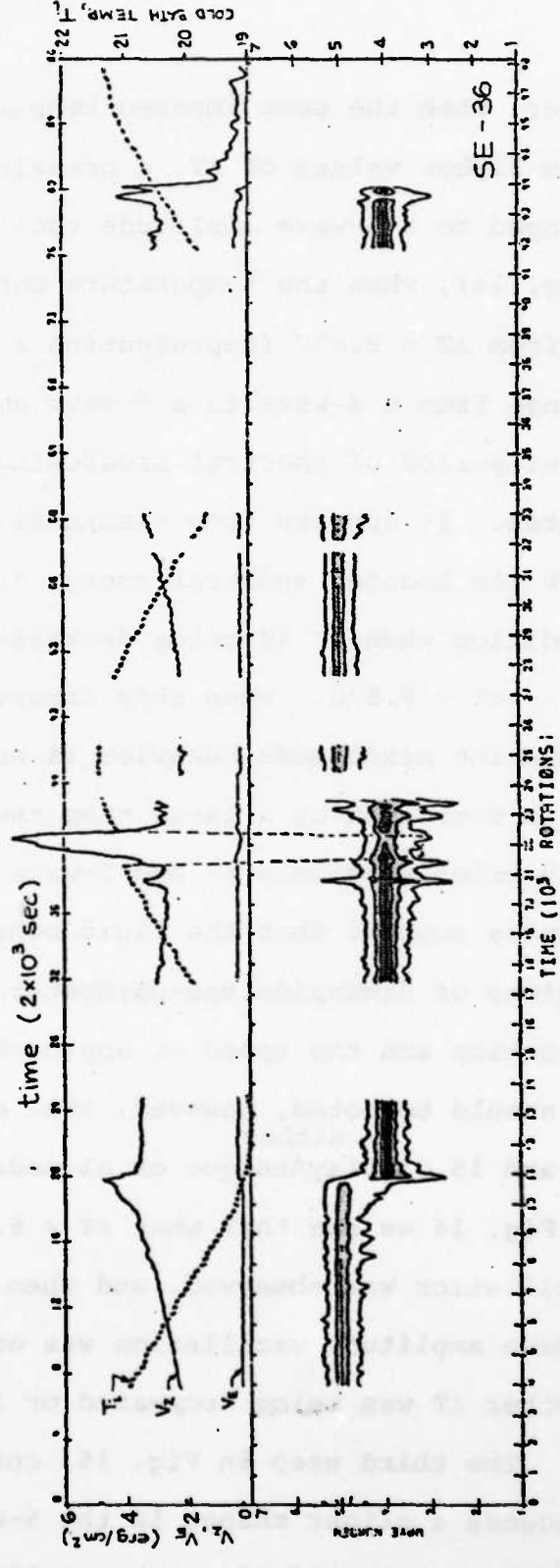


Fig. 16: Response of the temperature variance to a continuous variation of the cold bath temperature ΔT_c providing a corresponding variation of the imposed temperature contrast over the range 8.1 ΔT_c 10.5°C in experiment SE-36, series F. The cycle period is the same as that in experiment SE-35. The gaps in the record are due to intermittent failures in the data acquisition system while the imposed parameters of the experiment continued their prescribed course without interruption. A temporary failure in the thermostatic control of the cold-bath temperature caused this temperature to decrease by approximately 4.5°C for approximately 1000 rotations in the vicinity of $t = 22,000$ rot. It is interesting that the variance spectrum was not radically altered during this period. The rapid decline in V_z and V_e after $t = 43,000$ rot. is due to the fact that the turntable slowly came to a halt after this time.

Later, when the same imposed temperature contrast was approached from higher values of ΔT , a preexisting mixed-mode pattern changed to a 5-wave amplitude vacillation. In experiment SE-34 (Fig. 14), when the temperature contrast $\Delta T = 8.0^\circ\text{C}$ was approached from $\Delta T = 9.8^\circ\text{C}$ (representing a larger jump) there was a change from a 4-wave to a 5-wave amplitude vacillation with a brief period of spectral broadening separating the two wave states. It appears from examination of these two experiments that the broader spectral energy distribution is the preferred condition when ΔT is being decreased slowly in the interval $8.1 < \Delta T < 8.5^\circ\text{C}$. When this interval is traversed in small steps, the mixed-mode behavior is sustained (Fig. 15), but, when it is traversed by a large step, the mixed-mode behavior appears only briefly between 4- and 5-wave amplitude vacillation. These results suggest that the fluid behavior, at least in certain regions of dimensionless-parameter space, depends upon both the direction and the speed of approach from neighboring regions. It should be noted, however, that certain of the steps in Figs. 14 and 15 display ^{either} unique or bi-modal behavior. For example, in Fig. 14 we see that when $\Delta T = 6.7^\circ\text{C}$, only 5-wave amplitude vacillation was observed, and when $\Delta T = 9.8^\circ\text{C}$, either 4-wave or 5-wave amplitude vacillation was observed, depending upon whether ΔT was being decreased or increased.

The third step in Fig. 15, corresponding to $\Delta T = 9.2^\circ\text{C}$ produces a slight change in the 5-wave amplitude vacillation pattern. In particular, the amplitude of wave number 5 decreases

and the spectrum tends to broaden slightly toward lower wave numbers, suggesting that 5-wave amplitude vacillation is not as well established as it was in the preceding step. When a temperature contrast close to this value ($\Delta T = 9.3^\circ\text{C}$) is traversed from the opposite direction, a preexisting 4-wave amplitude vacillation is sustained during the entire step.

The fourth step, corresponding to $\Delta T = 10.1^\circ\text{C}$, produces a change from the 5-wave to a 4-wave amplitude vacillation in the interval $8,260 \leq t \leq 11,130$ rot; but much later during the second cycle ($32,130 \leq t \leq 34,830$ rot) the preexisting 5-wave amplitude vacillation is only weakened and the spectrum broadened slightly toward lower wave numbers when ΔT is changed from 9.1 to 10.0°C . When a temperature contrast close to this value ($\Delta T = 10.2^\circ\text{C}$) is traversed from the opposite direction during the time interval $14,220 \leq t \leq 17,090$ rot a preexisting 4-wave amplitude vacillation is seen to persist. The final step, corresponding to $\Delta T = 10.5^\circ\text{C}$ sustains the preexisting 4-wave amplitude vacillation during the first cycle and changes the 5-wave to a 4-wave amplitude vacillation during the second cycle. These results are consistent with those of Fig. 14.

In addition to the two experiments described above, we also ran an experiment (SE-36) in which ΔT was varied slowly and continuously over essentially the same range as in SE-35 with a 24-hour cycle period. Unfortunately, difficulties with our data system created large data gaps in the record. Nevertheless, it was considered worthwhile to present the results (Fig. 16)

because of their consistency with those shown in Fig. 15.

Fig. 17 is a schematic diagram encompassing the results of the hysteresis experiments presented in Figs 14, 15, and 16. We may summarize these results as follows: When Ω is held constant at 1.718 sec^{-1} and ΔT is changed sufficiently slowly that the fluid has ample time to adjust to each new imposed temperature contrast, 5-wave amplitude vacillation is the dominant characteristic in the interval $6.6 < \Delta T < 8.0^\circ\text{C}$ regardless of whether ΔT is being increased or decreased through this interval. The 5-wave amplitude vacillation will sustain itself if ΔT is increased in the interval $8.0 < \Delta T < 10.1^\circ\text{C}$, but will change to a dominant 4-wave amplitude vacillation when ΔT exceeds 10.1°C . The 4-wave amplitude vacillation will prevail if ΔT is brought back in steps to 8.5°C and will change to a mixed mode amplitude vacillation in the interval $8.5 > \Delta T > 8.0^\circ\text{C}$ before changing to the dominant 5-wave amplitude vacillation which is characteristic of the interval $6.6 < \Delta T < 8.0^\circ\text{C}$. When ΔT is lowered further the 5-wave amplitude vacillation persists until $\Delta T \rightarrow 6.1^\circ\text{C}$ at which time a mixed mode amplitude vacillation develops. As ΔT is raised again this pattern is preserved until $\Delta T \rightarrow 6.6^\circ\text{C}$ at which time the pattern returns to a dominant 5-wave amplitude vacillation. Thus, the history of the flow determines the observed flow pattern in the range $6.1 < \Delta T < 10.6^\circ\text{C}$, except within the interval $6.5 < \Delta T < 8.0^\circ\text{C}$ where wave number 5 is observed to dominate whether ΔT is being increased or decreased. Similar behavior can be expected in other regions of dimensionless-parameter

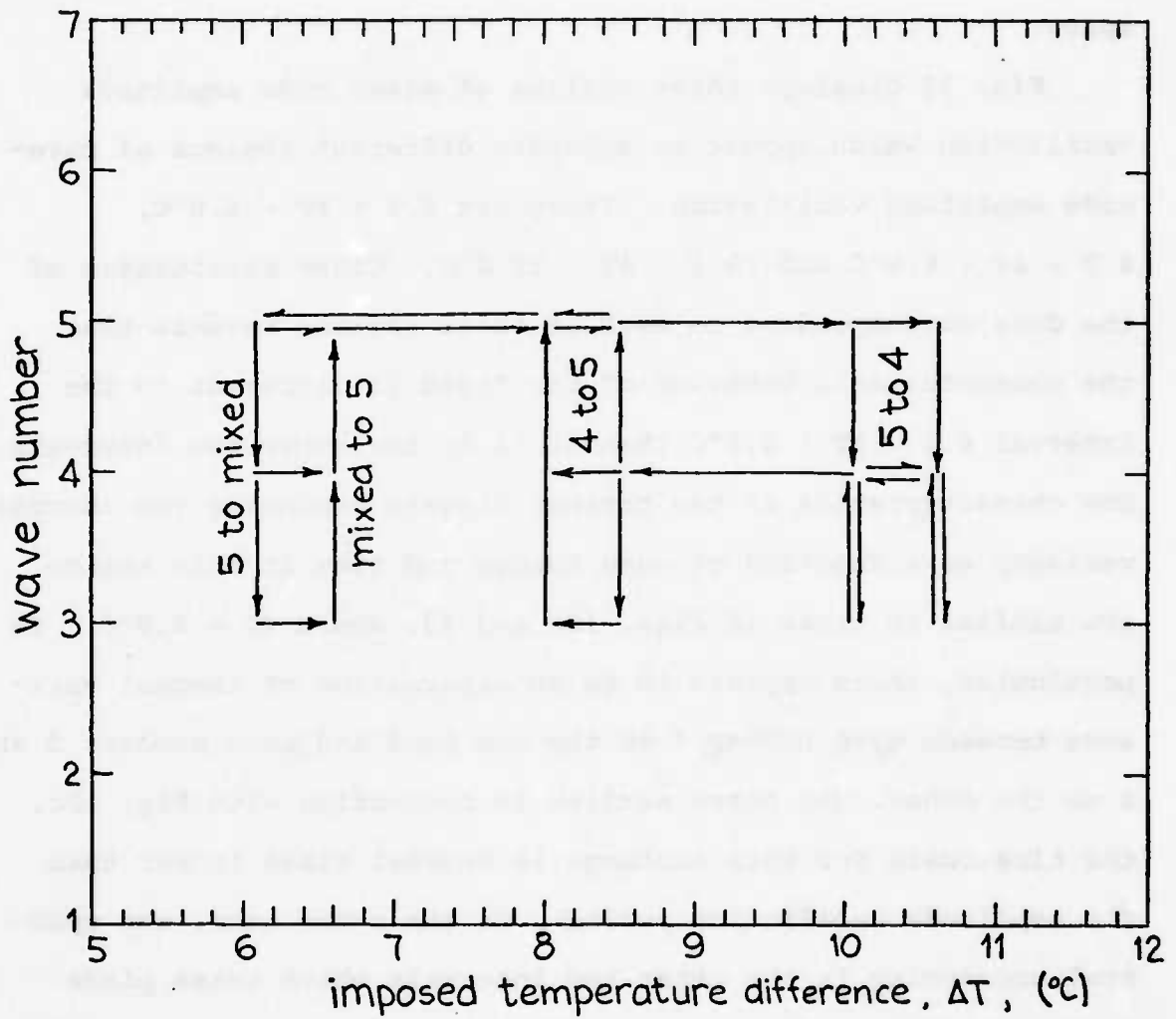


Fig. 17: Schematic diagram summarizing the results of the hysteresis experiments SE-34, 35 and 36 shown in the preceding three figures. The dominant modes present in the flow field are indicated as a function of the imposed temperature contrast, ΔT , and its direction of change.

space.

Fig. 17 displays three regions of mixed mode amplitude vacillation which appear to separate different regions of pure-mode amplitude vacillation. These are $6.1 < \Delta T < 6.6^\circ\text{C}$, $8.0 < \Delta T < 8.5^\circ\text{C}$ and $10.1 < \Delta T < 10.6^\circ\text{C}$. Close examination of the data corresponding to each of these regions reveals that the characteristic behavior of the fluid is different in the interval $6.1 < \Delta T < 6.6^\circ\text{C}$ than it is in the other two intervals. The characteristics of the contour diagram depicting the thermal variance as a function of wave number and time in this region are similar to those in Figs. 12c and 13, where $\Delta T = 5.9^\circ\text{C}$. In particular, there appears to be an alternation of thermal variance between wave number 5 on the one hand and wave numbers 3 and 4 on the other. (As noted earlier in connection with Fig. 12c, the time-scale for this exchange is several times longer than the amplitude vacillation period). On the other hand, the spectral broadening in the other two intervals which takes place either briefly or for a sustained period of time during wave-number changes from 4 to 5 or from 5 to 4 displays the *simultaneous* presence of all three modes.

10. Cyclic variations of the imposed temperature contrast

Ten experiments were conducted with cyclic variations of the imposed temperature contrast. These are included within series A, B, C, D, and E in Table 1 and in Fig. 1. In each experiment a null state was established first, corresponding either to the

maximum or minimum temperature contrast in the cycle. Next, the temperature contrast was varied cyclically between specified limits. The shortest experiment comprised 5 cycles; the longest, 50 cycles. Cycle periods used were 2, 1 and 0.5 hours, covering a range of periods from 2516 to 492.1 rot. The lengths of the cycles were from 8 to 57 times longer than the amplitude vacillation periods (see Table 2) and from 4 1/2 to 9 times longer than the average ^{thermal} lag time of the fluid at mid-radius.

In interpreting the results of these experiments we shall make frequent reference to Fig. 17. This figure reveals that, when ΔT is changed slowly in the range $6.1 \leq \Delta T \leq 10.6$ C, the possible modes of behavior in each of five intervals are limited and predictable as a function of ΔT . With the use of definitions introduced into the meteorological literature by Lorenz (1968), the behavior of the fluid would be characterized as transitive within the interval $6.6 < \Delta T < 8.0^\circ\text{C}$ and intransitive outside this interval. A flow is said to be transitive if its long-time-averaged statistics are independent of the initial state, and intransitive if its long-time-averaged statistics depend upon the initial state. In the interval $6.6 < \Delta T < 8.0^\circ\text{C}$, five-wave amplitude vacillation occurred whether the imposed temperature contrast was being increased or decreased. Outside this interval, the observed flow configuration depended upon the direction from which the imposed temperature contrast was approached.

Both transitive and intransitive flows are *determinate* in

the sense that both are predictable once the finite amplitude flow becomes sufficiently well established. When ΔT is cycled more rapidly through the same range, however, the fluid may not have adequate time to respond fully to the changing conditions.

A well-established flow configuration might, therefore, be sustained through portions of the cycle in which the imposed conditions are otherwise unfavorable for its development. Moreover, a flow pattern which is poorly established because of the rapidity with which the imposed conditions passed through the interval most favorable for its development might easily be upset and replaced by another pattern even before reaching the limit indicated in Fig. 17 for the onset of that pattern. As a result of such possibilities, the fluid could display different behavioral characteristics at the same stage of different imposed cycles, depending upon how well established the pattern is as it enters each stage. We shall characterize such behavior as *indeterminate*. We shall define a flow as *indeterminate* if, by virtue of its own internal non-linear dynamics, the time series of any significant parameter describing the flow can alternate sporadically between two or more characteristic flow configurations. "Almost intransitive" flow, as defined by Lorenz (1968), can be considered to be a special case of *indeterminate* flow in which given flow configurations last for long time periods in

comparison with the characteristic time scales of the fluid.

On average, it is reasonable to expect that the faster we cycle the imposed temperature difference through the prescribed range, the greater will be the lag between it and the internal gradient of the zonally-averaged temperature (measured as a percentage of the cycle time), and the smaller will be the excursion of the internal temperature gradient, $\partial\bar{T}/\partial R$, from its time-mean value. In a particular phase of a particular cycle, however, the actual radial temperature distribution in the interior of the fluid will depend also upon the nature of the convective processes present during that phase of the cycle under consideration. For example, when ΔT is intensified, $\partial\bar{T}/\partial R$ will tend to increase faster in the presence of a wave pattern which is inefficient in transporting heat "poleward" than it would in the presence of one which is more efficient. In an *indeterminate* system, $\partial\bar{T}/\partial R$ could be strong or weak at the same phase of different imposed cycles, depending upon which wave scale dominates and how well-established it is when it enters this phase of each cycle. In the presence of an inefficient wave pattern, $\partial\bar{T}/\partial R$ could increase to the point of baroclinic instability for the formation of a new, more efficient, wave pattern, after which it would decrease more rapidly than would be expected from simple arguments concerning the response of the fluid to the cyclic variation of ΔT . Irregularities in the behavior of $\partial\bar{T}/\partial R$ in the interior of the fluid that would be implied by such behavior were observed in the data (see, for example, Fig. 10b).

Because of the strong relationship between $\partial\bar{T}/\partial R$ and V_z , the existence of such irregularities is reflected also in the curves depicting the time variation of V_z to be presented in this section.

We consider first the experiments in series A, all of which were conducted at $\Omega = 1.718 \text{ sec}^{-1}$. The experiment with the longest cycle-period in this series (viz., 1968 rot) was SE-29. Fig. 18 shows contours of thermal variance as a function of wave number and time, and curves of V_z and V_E as a function of time, corresponding to this experiment. Initially, the cold-bath temperature was sustained at its highest value in this experiment, producing the minimum imposed temperature contrast, 5.9°C . The flow during this time interval was an alternating mixed-mode amplitude vacillation similar to that found in SE-25 (Fig. 12c) and in the first part of SE-32 (Fig. 13), during which $\Delta T = 5.9^\circ\text{C}$. Such behavior was also observed in the hysteresis experiment, SE-34 (Fig. 14), while the imposed temperature contrast was undergoing intensification in the interval $6.1 \leq \Delta T \leq 6.6^\circ\text{C}$.

After the initial sustained "summer" condition, the imposed temperature difference between the cold and hot baths was cycled in the range $5.9 \leq \Delta T \leq 10.6^\circ\text{C}$. The contour diagram for this experiment displays at different times the various characteristics of the temperature spectra observed in the hysteresis experiments and summarized in Fig. 17. In particular, the diagram reveals time intervals with predominantly 5-wave and

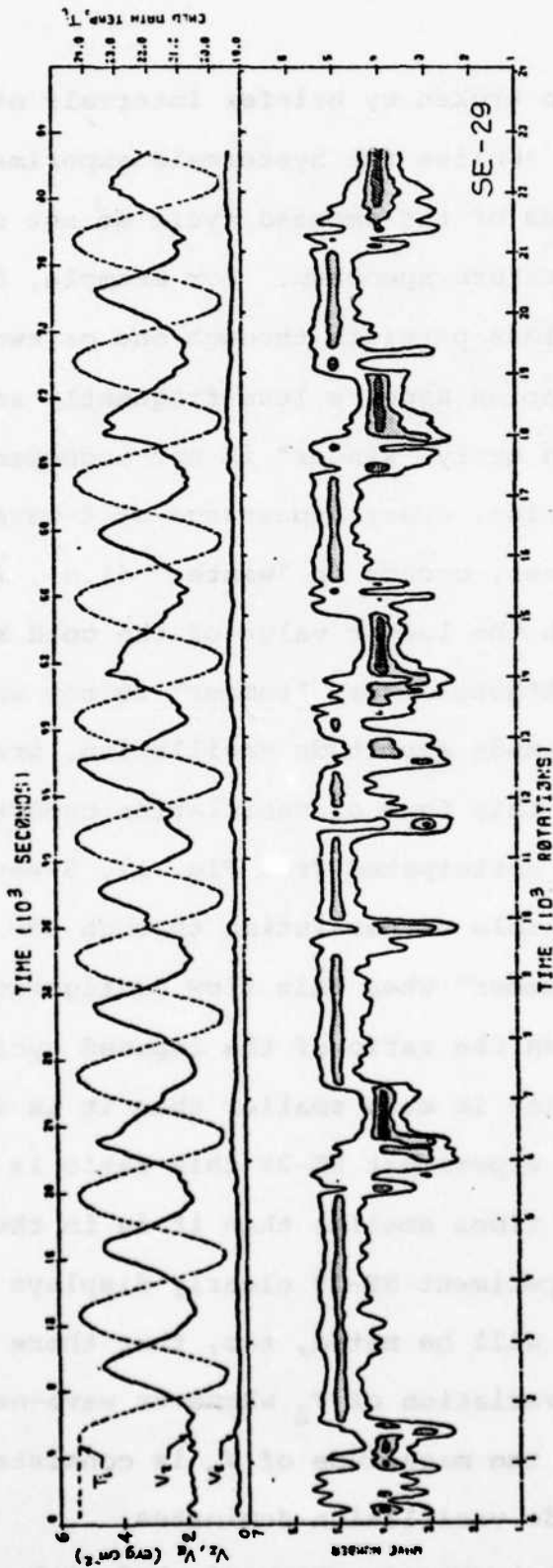


Fig. 18: Response of the temperature variance to 2-hour cyclic variations of the cold inner-bath temperature over a 4.6°C range, providing imposed temperature contrasts from 5.9 to 10.5°C in experiment SE-29, series A. Quantities represented and contour values and intervals are the same as in Figs. 12-16. In this, and in all other cyclic experiments to be described, the vertical stratification used in calculating the energy equivalents of V_z and V_g was determined using the time average of $[(T_{1/6})^{3/4} - (T_{1/6})^{1/2}]$ over the cyclic portion of the experiment starting with the second cycle and continuing for the maximum integral number of cycles possible.

4-wave amplitude vacillation broken by briefer intervals of mixed-mode amplitude vacillation. Unlike the hysteresis experiments, however, corresponding phases of the imposed cycle do not necessarily yield the same temperature spectrum. For example, 5-wave amplitude vacillation sometimes persists through one or two cycles, and 4-wave amplitude vacillation appears less frequently and for shorter durations. Although every "winter" is not accompanied by 4-wave amplitude vacillation, every appearance of 4-wave amplitude vacillation, however, occurs in "winter" (i.e., in the quarter cycle beginning with the lowest value of the cold bath temperature). Similarly, although every "summer" is not accompanied by alternating mixed-mode amplitude vacillation, practically every appearance of this form of vacillation occurs in "summer". As we might have anticipated from Fig. 17, 5-wave amplitude vacillation is capable of persisting through the extremes of "winter" and "summer" when this flow configuration is well established, and when the ratio of the imposed cycle period to the thermal lag time is much smaller than it is in the hysteresis experiments. In experiment SE-29 this ratio is 8.4 which is of the order of 10 times smaller than it is in the hysteresis experiments. Experiment SE-29 clearly displays *indeterminate* behavior. It will be noted, too, that there are irregularities in the time variation of V_z whenever wave-number changes take place and that the magnitude of V_E is consistently smaller when 5-wave amplitude vacillation dominates.

It might be expected that experiments conducted with a

higher frequency of cycling within the same limits of imposed ΔT , and at the same value of Ω , would display even more erratic behavior, with the internal non-linear dynamics of the flow exerting greater control over events and the particular phase of the imposed cycle playing a smaller role. In this connection, we may examine the results of experiments SE-23, 24, and 26 (Figs. 19, 20, and 21, respectively) in which the imposed cycle period was 984.1 rot, with $\Omega = 1.718 \text{ sec}^{-1}$, and ΔT was varied over the intervals $6.1 \leq \Delta T \leq 10.6^\circ\text{C}$, $5.9 \leq \Delta T \leq 10.4^\circ\text{C}$ and $5.6 \leq \Delta T \leq 10.2^\circ\text{C}$, respectively. The control parameters were sufficiently close to justify considering these experiments together as a group. Although our data acquisition system malfunctioned on several occasions during each experiment, leaving periods of missing data, there is an ample amount of information on which to derive conclusions. The most striking feature observed upon comparing the results of the three experiments is the fact that, although 5-wave amplitude vacillation is interrupted by other modes of behavior on several occasions during experiments SE-23 and SE-26, this phenomenon continues uninterrupted through 19 of the 20 "annual" cycles in experiment SE-24. We can only speculate that the 5-wave amplitude vacillation in SE-24 was more firmly established than was the case in the other two experiments and, in spite of numerous tendencies toward spectrum broadening, a condition which usually precedes wave number changes, was never sufficiently unstable for the formation of another wave pattern. In any case, it is evident that

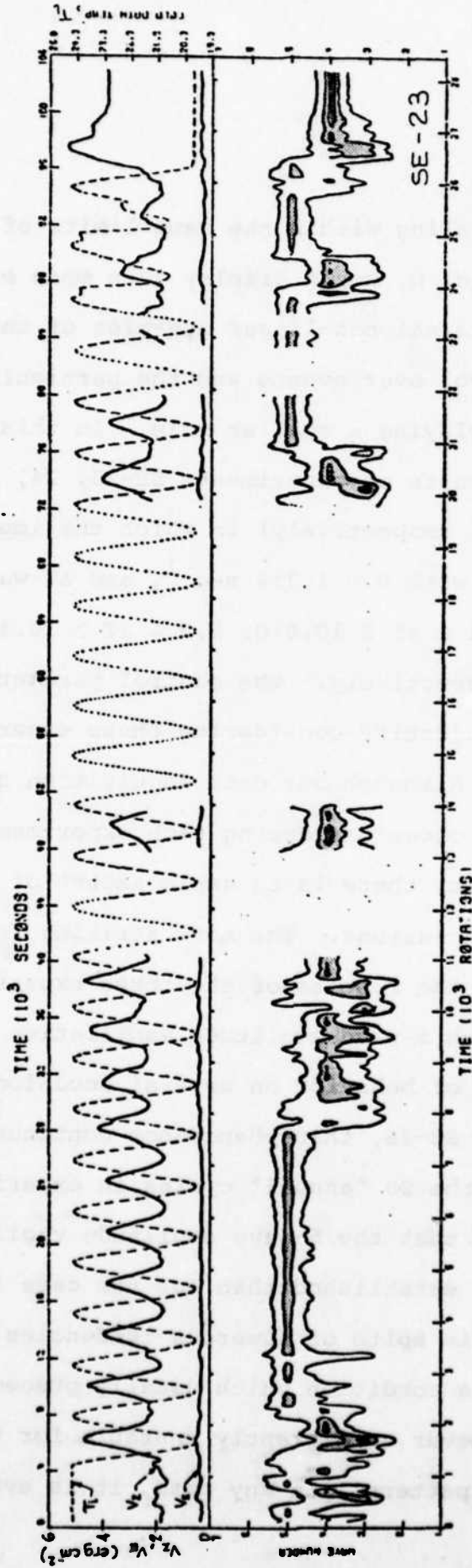


Fig. 19: Response of the temperature variance to 1-hour cyclic variations of the cold inner-bath temperature over a 4.5°C range, providing imposed temperature contrasts from 6.1 to 10.6°C in experiment SF-23, series A ($\Omega = 1.718 \text{ sec}^{-1}$). Gaps in the record are due to intermittent failures in the data acquisition system while the imposed parameters of the experiment continued their prescribed course without interruption. The remaining comments are the same as in Fig. 18.

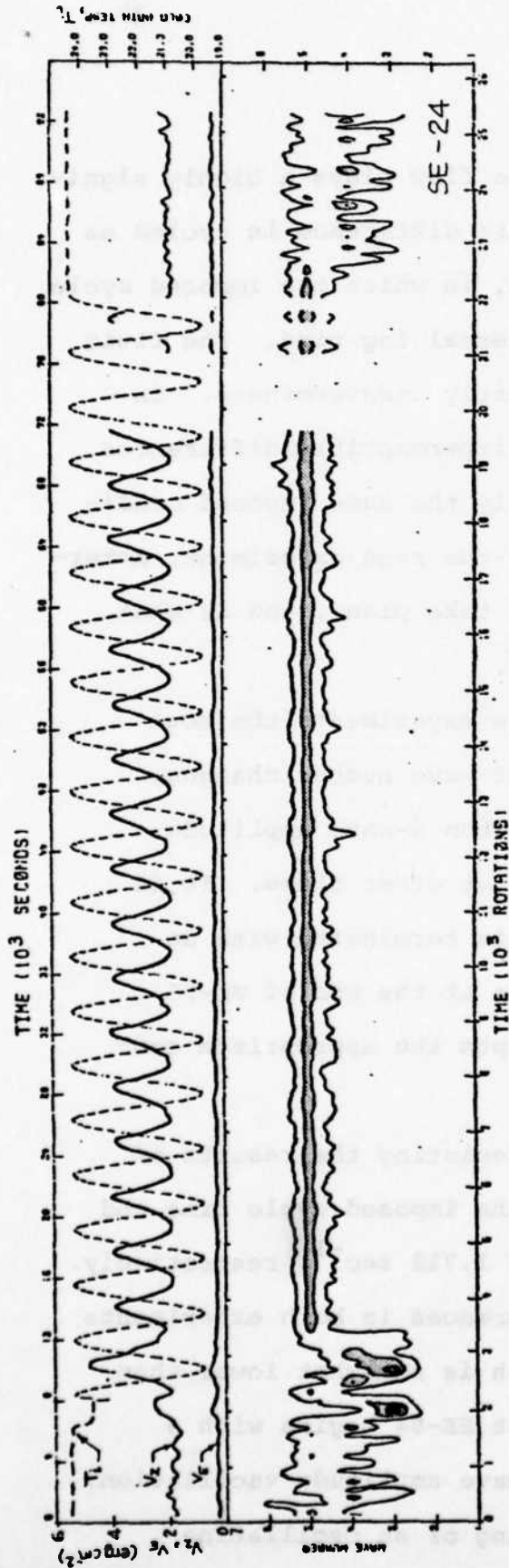


Fig. 20: Response of the temperature variance to 1-hour cyclic variations of the cold inner-bath temperature over a 4.5°C range, providing imposed temperature contrasts from 5.9 to 10.4°C in experiment SE-24 series A ($\Omega = 1.718 \text{ sec}^{-1}$). The remaining comments are the same as in Figs 18 and 19.

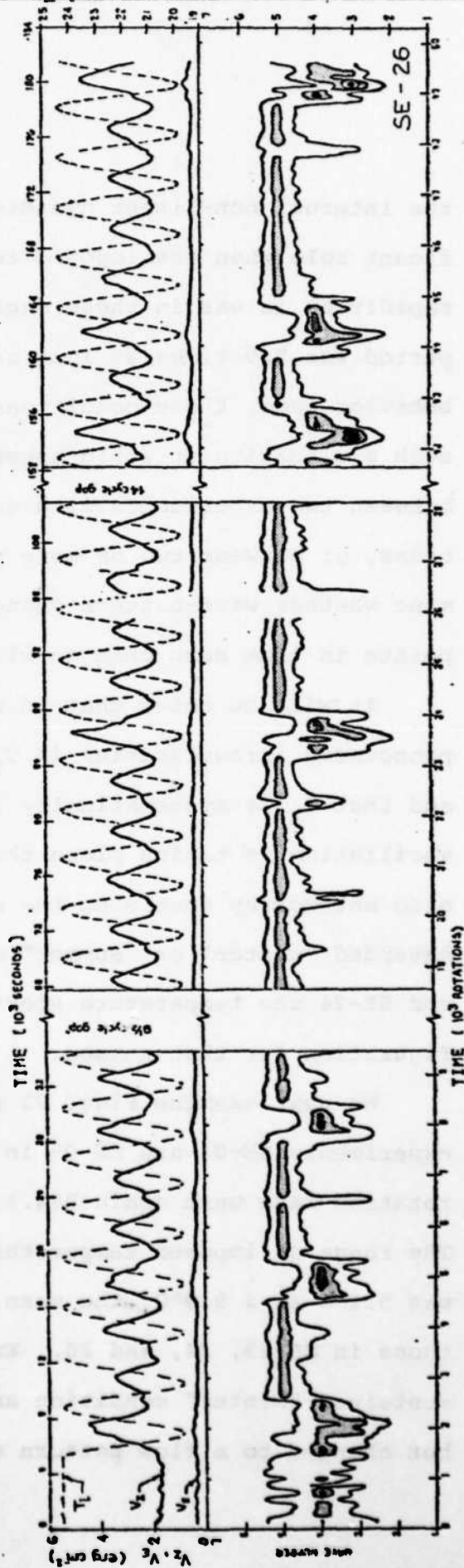


Fig. 21: Response of the temperature variance to 1-hour cyclic variations of the cold inner-bath temperature over a 4.6°C range, providing imposed temperature contrasts from 5.6 to 10.2°C in experiment SE-26, series A ($\Omega = 1.718 \text{ sec}^{-1}$). The remaining comments are the same as in Figs. 18 and 19.

the internal non-linear dynamics of the flow plays a highly significant role when the imposed temperature difference is cycled as rapidly as it was in these experiments, in which the imposed cycle period was 5.5 times as long as the thermal lag time. The fluid behavior under these conditions is clearly *indeterminate*. In such a situation it would appear that imperceptible differences between two experiments with essentially the same imposed conditions, or between two or more parts of the same experiment, determine whether wave-pattern changes will take place, and at what points in time such changes will occur.

It will be noted that in all three experiments the most pronounced irregularities in V_z reflect wave number changes, and that V_E is systematically smaller when 5-wave amplitude vacillation is taking place than it is at other times. It is also noteworthy that when the cycling is terminated with an extended "winter" or "summer" condition at the end of SE-23 and SE-24 the temperature spectrum adopts the appropriate configuration for that season.

We next examine Figs. 22 and 23 depicting the results of experiments SE-04 and SE-05 in which the imposed cycle time and rotation rate were again 984.1 rot and 1.718 sec^{-1} , respectively. The range of imposed temperature differences in both experiments was $5.2 \leq \Delta T \leq 9.9^\circ\text{C}$, the mean of which is somewhat lower than those in SE-23, 24, and 26. Experiment SE-04 begins with a sustained "winter" condition and a 4-wave amplitude vacillation, but changes to a flow pattern consisting of an oscillating

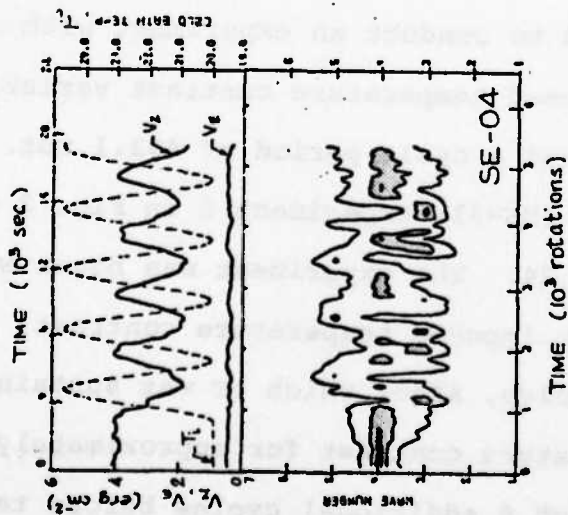


Fig. 22

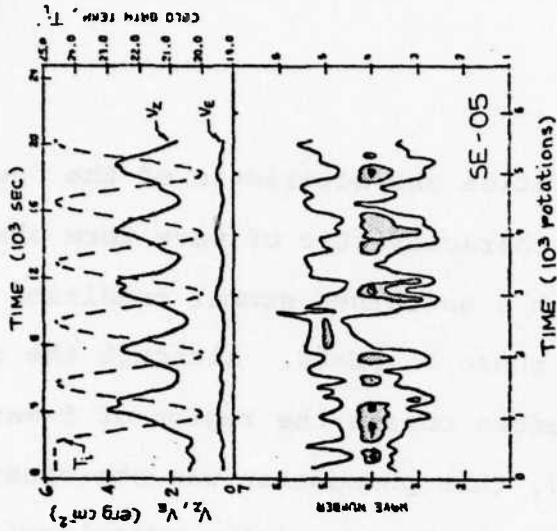


Fig. 23

Figs. 22 & 23: Response of the temperature variance to 1-hour cyclic variations of the cold inner-bath temperature over a 4.7°C range, providing imposed temperature contrasts from 5.2 to 9.9°C in experiments SE-04 and SE-05, series A ($\Omega = 1.718 \text{ sec}^{-1}$). The only difference between the two experiments is that the initial condition for SE-04 is a "winter" condition, while that for SE-05 is a "summer" condition. The remaining comments are the same as in Figs. 18 and 19.

mixed-mode amplitude vacillation characteristic of the "summer" flows and a broad spectrum characteristic of wave form changes. Experiment SE-05 begins with a sustained summer condition and has characteristics similar to those in SE-04. Although the range of imposed temperature differences covers the region of 5-wave amplitude vacillation in Fig. 17, this phenomenon was not observed for any sustained period of time during either experiment. In the course of alternations of variance between wave number 5 on the one hand and 3 and 4 on the other, the lowest value of V_E occurred during the presence of the 5-wave vacillating pattern.

The series A experiments were performed with two different cycle periods of T_i (1968 and 984.1 rot). An experiment with a shorter cycle period within the same limits was attempted but was unsuccessful due to the relatively large thermal mass of the inner bath fluid and the high heating and cooling rates required. Accordingly, it was decided to conduct an experiment with a reduced amplitude of the imposed temperature contrast variation (viz., $7.8 \leq \Delta T \leq 10.0^\circ\text{C}$) and a cycle period of 492.1 rot. The results of this experiment (SE-31; experiment B in Fig. 2 and Table 1) are shown in Fig. 24. The experiment was begun with a sustained period of maximum imposed temperature contrast, followed by 36 "annual" cycles, after which ΔT was sustained at the minimum imposed temperature contrast for approximately 2200 rot and then carried through 8 additional cycles before terminating the experiment. The dashed line above the contour diagram depicting the variation of T_i reveals that, at this high

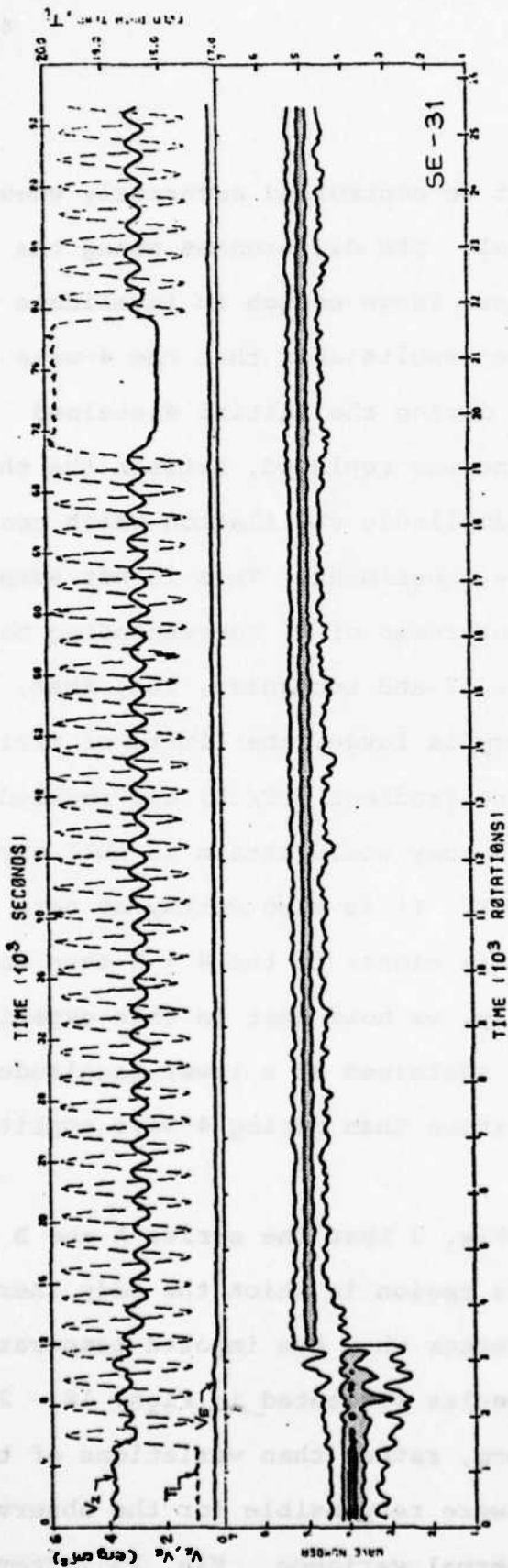


Fig. 24: Response of the temperature variance to 1/2-hour cyclic variations of the cold inner-bath temperature over a 2.2°C range, providing imposed temperature contrasts from 7.8 to 10.0°C in experiment SE-31, series B ($\Omega = 1.718 \text{ sec}^{-1}$). A temporary failure in the thermostatic control of the cold bath temperature caused the temperature contrast to remain at 7.8°C for approximately 2200 rot after the completion of 36 imposed cycles. The remaining comments are the same as in Figs. 18 and 19.

cycling frequency, T_c , could not be controlled accurately enough to make all the cycles identical. The differences among the various cycles were not, however, large enough to invalidate the data from this experiment. The results show that the 4-wave amplitude vacillation, which formed during the initial sustained "winter" condition, weakened and was replaced, between the third and fourth cycle, by a 5-wave amplitude vacillation which continued for the remainder of the experiment. This is not surprising when we examine where the extremes of ΔT corresponding to this cycle lie relative to Fig. 17 and recognize, too, that, when the imposed cycle frequency is large, the limits of variation of the internal temperature gradient ($\bar{\partial T / \partial R}$) are reduced considerably from the magnitude they would attain in null experiments at the two extremes of ΔT . It is also worthy of note that the mean ΔT of this experiment is closer to the 4 \rightarrow 5 than to the 5 \rightarrow 4 transition point. Finally, we note that in this experiment, as in the preceding ones, V_E is sustained at a lower magnitude during 5-wave amplitude vacillation than during 4-wave amplitude vacillation.

It will be recalled from Fig. 3 that the series A and B experiments were conducted in a region in which the eddy thermal variance is not necessarily greater when the imposed temperature difference is greater. The results presented in Figs. 18 - 24 reveal that changes in wave-form, rather than variations of the imposed temperature contrast, were responsible for the observed time variations of the eddy thermal variance. Fig. 25 (after

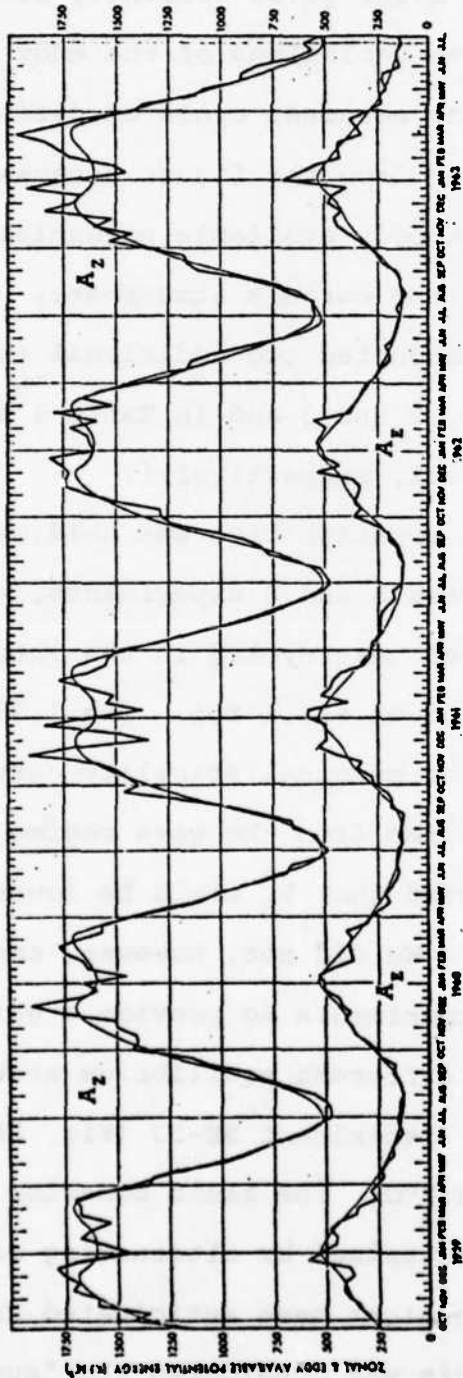


Fig. 25: Variation of 10-day averages of zonal (AZ) and eddy (AE) available potential energy for the layer 850-500 mb (heavy curve) in the earth's atmosphere for the period October 1958-July 1963. The light curve is the same for each year and represents averages of the monthly values for the five years of data (after Krueger, Winston and Haines, 1965).

Winston, Krueger and Haines, 1965) gives evidence, however, that in the earth's atmosphere time variations of the eddy thermal variance are controlled by the seasonal cycle of differential heating. This may be inferred from the figure because of the high time correlation between eddy available potential energy and eddy thermal variance in the earth's atmosphere. In order to simulate this effect, we conducted two additional experiments which are designated in Figs. 2 and 3 and in Table 1 as experiments C and D (SE-33 and SE-22, respectively).

In experiment SE-33 the rotation rate was held constant at the same value as in the series A and B experiments, but the imposed temperature difference was cycled in the interval $1.3 \leq \Delta T \leq 5.7^\circ\text{C}$ over a period of 984.1 rot. The 1.3°C extreme is believed to be close to the marginal stability curve separating the lower symmetric regime from the wave regime (Fig. 3). Accordingly, it was anticipated that V_E would be lowest in the "summer" phase of the cycle. We did not, however, conduct null experiments or hysteresis experiments to provide a guide to the wave-forms corresponding to different equilibrium states within the range $1.3 \leq \Delta T \leq 5.7^\circ\text{C}$. Experiment SE-33 (Fig. 26) was begun with ΔT sustained at 5.7°C . The fluid behavior during this time interval was characterized by alternating mixed-mode amplitude vacillation, as we might have anticipated from Fig. 17. In the type A experiments this was considered the "summer" condition. In the present experiment it is the "winter" condition, since the largest imposed temperature contrast in this experiment

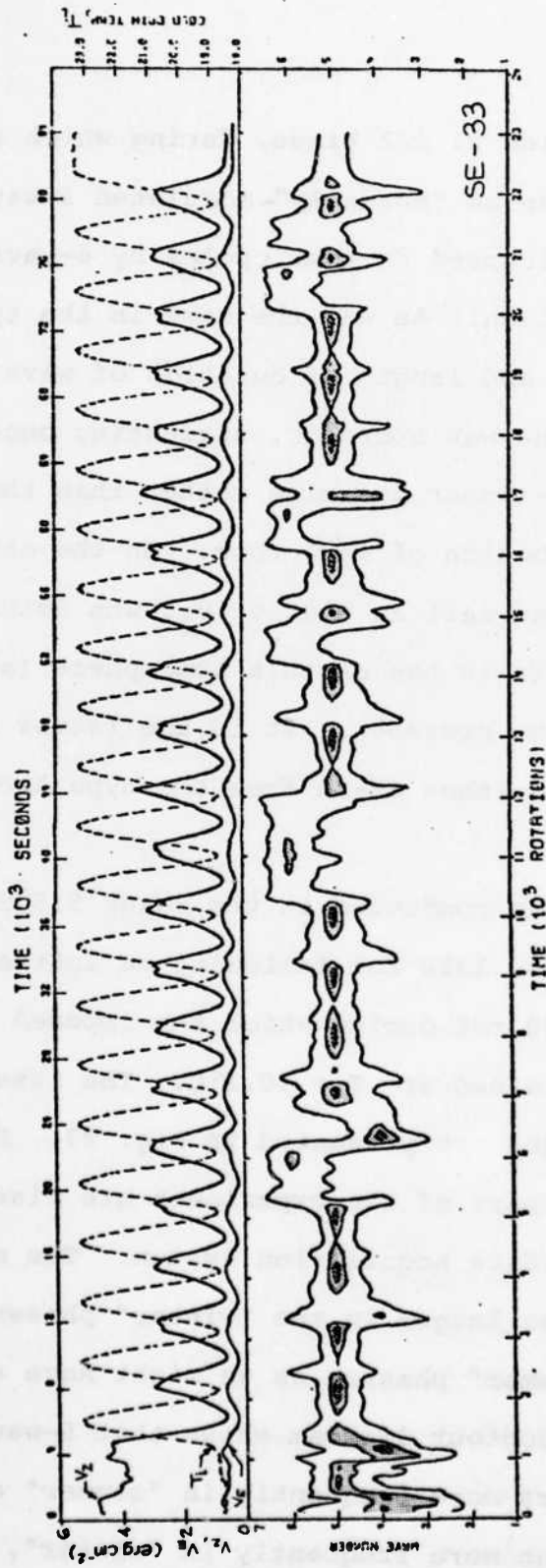


Fig. 26: Response of the temperature variance to 1-hour cyclic variations of the cold inner-bath temperature over a 4.4°C range, providing imposed temperature contrasts from 1.3 to 5.7°C in experiment SE-33, series C ($\Omega = 1.718 \text{ sec}^{-1}$). The location of this experiment in dimensionless-parameter space is shown in Figs. 2 and 3. The remaining comments are the same as in Fig. 18, except the contour intervals and their shadings are: from 0.005 to 0.020 °C² ; from 0.020 to 0.035 °C² ; and from 0.035 to 0.050 °C² .

was 5.7°C . T_i was then cycled $21\frac{1}{2}$ times, during which the prevailing fluid behavior was an "annually"-modulated 5-wave amplitude vacillation, interrupted in some cycles by 6-wave or 4-wave amplitude vacillation. As was the case in the type A experiments, the appearance and length of duration of wave forms other than the prevailing one was sporadic, suggesting once again that the internal non-linear dynamics rather than the "season" controlled the selection of wave form. On the other hand, the magnitude of V_E , as well as that of V_Z , was determined mainly by the season as it is in the earth's atmosphere (although wave-form influences are also present). It is the latter feature, in particular, which distinguishes SE-33 from the type A experiments.

Experiment D (SE-22) was conducted in the range $5.5 \leq \Delta T \leq 10.1^{\circ}\text{C}$ with a cycle period of 1320 rot following an initial period of approximately 1000 rot during which the imposed temperature contrast was maintained at $T = 10.1^{\circ}\text{C}$. The results pertaining to this experiment are presented in Fig. 27. Data corresponding to the early part of the experiment are missing because of failures in the data acquisition system. The measurements reveal that V_E was larger in the "winter" phases of the cycles than in the "summer" phases, as we might have anticipated from Fig. 3. The contour diagram shows that 5-wave amplitude vacillation occurs more frequently in "summer" and 4-wave amplitude vacillation more frequently in "winter", although there is sufficient intra-"annual" variability to

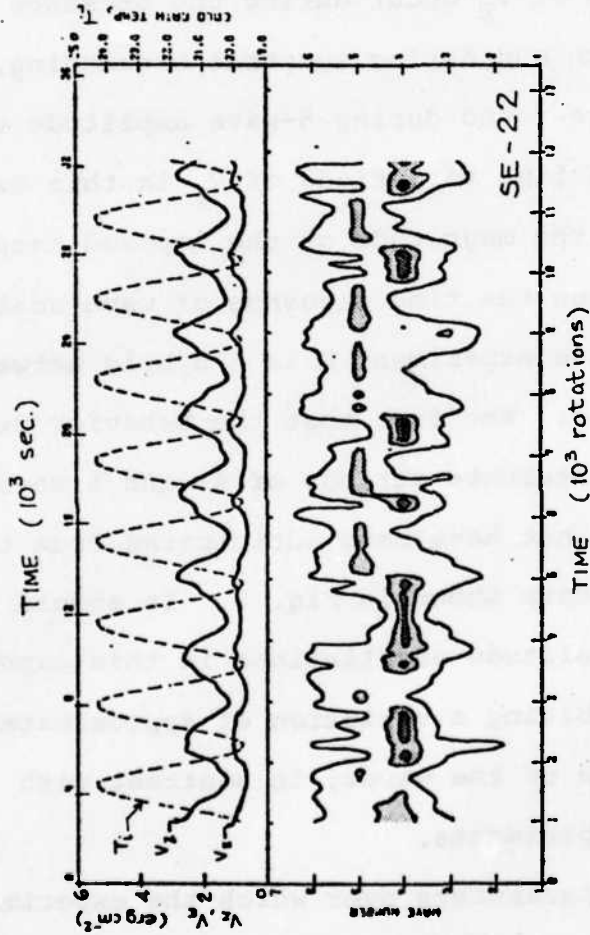


Fig. 27: Response of the temperature variance to 1-hour cyclic variations of the cold inner-bath temperature over a 4.6°C range, providing imposed temperature contrasts, from 5.5 to 10.1°C in experiment SE-22, series D ($\Omega = 2.304 \text{ sec}^{-1}$). The location of this experiment in dimensionless-parameter space is shown in Figs. 2 and 3. The remaining comments are the same as in Fig. 18, except the contour intervals and their shadings are: from 0.01 to 0.05°C² [white]; from 0.05 to 0.09°C² [light gray]; from 0.09 to 0.13°C² [dark gray]; and from 0.13 to 0.17°C² [black].

classify the fluid behavior as *indeterminate*. There is also a tendency for spectral broadening during "winter". The only time a given wave scale dominates through a full cycle is during the third "summer". During this period V_E is greater than normal. More generally, high values of V_E occur during the presence of 4-wave amplitude vacillation and during spectral broadening, whereas low values of V_E are found during 5-wave amplitude vacillation, suggesting that the time variations of V_E in this experiment depend not only upon the magnitude of the imposed temperature contrast, but also upon the time sequence of wave scales which develop. In this sense experiment D is a hybrid between the type A and C experiments. The fact that the behavior of the fluid is dominated by alternate periods of 4- and 5-wave amplitude vacillation would not have been anticipated from the results of the null experiments shown in Fig. 2. It should be noted, however, that the amplitude vacillations in this experiment were rather weak, exhibiting a variation of approximately 30% about the mean amplitude of the waves, in contrast with nearly 100% in the other experiments.

The range of external parameters over which the experiments were performed was expanded further by conducting experiment E (SE-30) with a larger excursion of the imposed temperature contrast (viz., $11.0 \leq \Delta T \leq 20.2^\circ\text{C}$). The rotation rate selected was $\Omega = 2.196 \text{ sec}^{-1}$. According to Fig. 3, V_E would not be expected to vary significantly as a function of ΔT . The results corresponding to this experiment, presented in Fig. 28, confirm

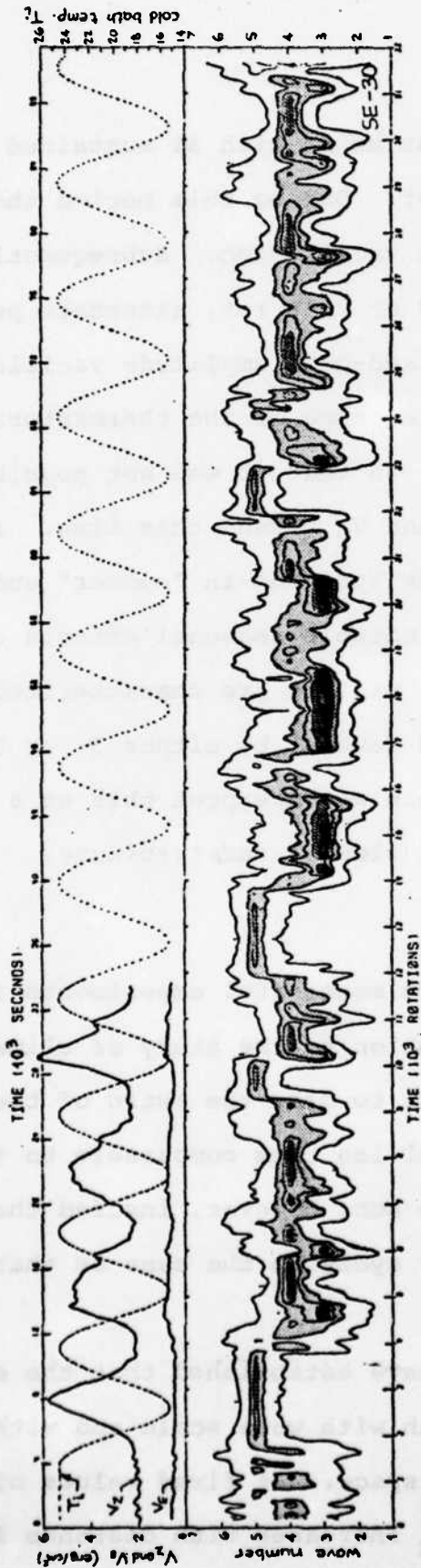


Fig. 28: Response of the temperature variance to 2-hour cyclic variations of the cold inner-bath temperature over a 9.2°C range, providing imposed temperature contrasts from 11.0 to 20.2°C in experiment SE-30, series E ($\Omega = 2.196 \text{ sec}^{-1}$). The location of this experiment in dimensionless-parameter space is shown in Figs. 2 and 3. The quantities V_z and V_x could not be determined beyond the fourth imposed cycle due to a failure in certain channels of the data acquisition system required for their calculation. The channel which records the cold-bath temperature also failed after the fourth cycle, but an independent record of its variation was obtained and is shown as a dotted curve in the figure. The remaining comments are the same as in Fig. 18, except the contour intervals and their shadings are: from 0.01 to 0.05°C² [□]; from 0.05 to 0.13°C² [▤]; from 0.13 to 0.21°C² [▥]; and from 0.21 to 0.29°C² [▧].

this expectation. The experiment began with ΔT sustained at 11.0°C for approximately 1200 rot. During this period the fluid displayed a mixed-mode amplitude vacillation. Subsequently, when ΔT was cycled with a period of 2516 rot, alternate periods of 5-wave, 4-wave, 3-wave and mixed-mode amplitude vacillation appeared. After the fourth cycle, some of the thermistors at radius $R = 5/6$ gap-width failed, so that it was not possible to obtain accurate measures of V_Z and V_E beyond this time. Except for the general broadening of the spectrum in "summer" and narrowing in "winter" there are no notable seasonal effects evident in the contour diagram. Several winters are characterized by 4-wave amplitude vacillation and several by either 3- or 5-wave amplitude vacillation. Once again we interpret this as a property which characterizes the flow as *indeterminate*.

11. Comments and conclusions

(1) In an effort to perform meaningful experiments from the standpoint of their contribution to the study of climatic variability, we have been careful to make the ratio of the imposed cycle period to the thermal lag time comparable to that in the earth's atmosphere. We have not, however, insured that the number of rotations per "annual" cycle be the same as that in the atmosphere.

(2) Our null experiments have established that the eddy thermal variance (V_E) varies both with wave scale and with position in dimensionless-parameter space. At fixed values of the imposed temperature contrast, V_E increases with distance from

the marginal stability curve. When two different wave scales are possible at a fixed point in dimensionless parameter space, the lower wave number possesses a larger thermal variance than the higher one. As a consequence of these properties the relative magnitudes of V_E in the "summer" and "winter" phases of cyclic experiments depend strongly upon the structure of the regime diagram in the region of dimensionless parameter space in which the experiments are conducted. In the earth's atmosphere, the large-scale eddies are observed to be more vigorous in winter than in summer. Our results suggest that this may be due to the particular location of the atmosphere in dimensionless-parameter space due to its special combination of differential heating and rotation.

(3) Our experiments have revealed that the phenomena to be expected in any region of dimensionless-parameter space depend upon the direction of approach, the particular hysteresis properties in that region of the regime diagram and the rate at which the externally imposed conditions are being changed. Null experiments and hysteresis experiments have been found to display *determinate* behavior at different points in dimensionless-parameter space. Cyclic experiments have been found to display *indeterminate* behavior. There is evidence to suggest that the behavior of the fluid in cyclic experiments tends toward that in null experiments in the limit of very rapid cycling, and toward that in hysteresis experiments in the limit of very slow cycling. At intermediate cycling rates the fluid behavior is

no longer predictable solely as a function of the externally imposed conditions, although some experiments displayed a statistical bias for certain types of flows in certain seasons.

(4) The experiments in this study were performed in the region of dimensionless-parameter space in which the spectrum of possible wave states is narrow. The range of cycle periods was also limited by the apparatus available at the time. A valuable follow-up to this experimental series would be one in which a broad range of cycle periods is employed in the region of geostrophic turbulence and in the boundary region between geostrophic turbulence and regular waves.

(5) Referring to the identity

$$\frac{\partial \bar{T}}{\partial R} \equiv (\text{isothermal slope}) \times \frac{\partial \bar{T}}{\partial z}$$

We may note one significant difference between atmospheric behavior and the behavior of the fluid in rotating annulus experiments. In the earth's atmosphere, time variations of the horizontal temperature gradient, and of the related horizontal temperature variance are associated with changes in the slope of the isotherms, with little variation observed in the space mean vertical stratification of the atmosphere. In the annulus experiments, on the other hand, such variations are accompanied by significant changes in the vertical stratification, with much smaller changes observed in the slope of the isotherms.

Acknowledgements

The writers have been stimulated in this work by discussions with Dr. Francis Bretherton and Mr. Robert McArthur. We have also benefitted from helpful comments by Professor Edward Lorenz. We are grateful, too, for the laboratory data assistance we have received from Mr. McArthur, and for the data processing and computational efforts of Mssrs. James Zarichny and James Merritt. The experiments were conducted under NOAA Grant 04-6-1-158-44053 and ONR Contract N 00014-76-C-0844. The interpretive work and manuscript writing was accomplished under ONR Contracts N 00014-76-C-0844 and N 00014-77-C-0265.

REFERENCES

- Buzyna, G., R. Kung, W. W. Fowlis, and R. L. Pfeffer, 1973: Measurement of time dependent heat flux in the interior of a rotating differentially heated fluid. AICHE Symposium Series, 70, No. 138, 17-22.
- Cole, R. J., 1971: Hysteresis effects in a differentially heated rotating fluid annulus. Quart. J. Roy Meteor. Soc., 97, 506-518.
- Fowlis, W. W., J. C. Buckley, and J. W. Ruppert, 1972: The measurement of flow direction, flow speed and temperature in a liquid using a miniaturized array of thermistor beads. Tech. Rept. 37, Geophysical Fluid Dynamics Institute, Florida State University.
- Fultz, D., R. R. Long, G. V. Owens, W. Bohan, R. Kaylor, and J. Weil, 1959: Studies of thermal convection in a rotating cylinder with some implications for large-scale atmospheric motions. Meteor. Monogr., 4, No. 21.
- Kaiser, J. A. C., 1970: Rotating deep annulus convection. Part 2. wave instabilities, vertical stratification, and associated theories. Tellus, 22, 275-287.
- Krueger, A. F., J. S. Winston, and D. A. Haines, 1965: Computation of atmospheric energy and its transformation for the northern hemisphere for a recent five-year period. Mon. Wea. Rev., 93, 227-238.

Lacher, R. C., R. McArthur, and G. Buzyna, 1977: Catastrophic changes in circulation flow patterns. American Scientist, (in press).

Lorenz, E. N., 1968: Climatic determinism. Meteor. Monogr., 8, No. 30, 1-3.

Pfeffer, R. L., G. Buzyna, and W. W. Fowles, 1974: Synoptic features and energetics of wave-amplitude vacillation in a rotating, differentially-heated fluid. J. Atmos. Sci., 31, 622-645.

Snyder, H. A. and E. M. Youtz, 1969: Transient response of a differentially heated rotating annulus. J. Atmos. Sci., 26, 96-99.

**THIS PAGE IS BEST QUALITY PRACTICABLE
FROM CO. Y FURNISHED TO DDG**

*Reprinted from AMERICAN SCIENTIST, Vol. 65, No. 5, September-October 1977, pp. 614-621
Copyright © 1977 by Sigma Xi, The Scientific Research Society of North America Incorporated*

**THIS PAGE IS BEST QUALITY PRACTICABLE
FROM COPY FURNISHED TO DDG**

R. C. Lacher
Robert McArthur
George Buzyna

Catastrophic Changes in Circulation Flow Patterns

Catastrophe theory offers new insight into fundamental processes underlying laboratory simulation of abrupt changes in large-scale atmospheric circulation patterns

A heightened awareness of the impact of changes in circulation patterns of the upper atmosphere on surface climate has renewed interest in laboratory simulation of certain aspects of these phenomena. The relatively simple geophysical flows generated in a laboratory annulus, a ring-shaped open trough, have been extremely useful in identifying and studying some of the basic mechanisms of these changes in a controlled setting. Such experiments are generally conducted by subjecting a fluid within the annulus to a series of carefully controlled shifts in temperature contrast and rotation rate. The flows that result cover a broad spectrum ranging from radially symmetric to turbulent. These flows generally exhibit fast motion in a narrow band of the fluid when viewed from above and are usually classified according to the

wavelike pattern formed by this fast stream. Results are commonly represented by "regime diagrams" whose coordinates are proportional to the externally imposed temperature contrast and rotation rate. The regime diagrams show the boundary between the symmetric flow and wave flow "regimes" and are characterized by regions of particular wave forms, abrupt changes in wave form between different regions, and extensive hysteresis or delay in the points of transition between these regions. Thus such diagrams demonstrate the full range of stationary-state flow patterns of the system.

Laboratory experiments designed to simulate seasonal variations require a continuous and periodic variation of the imposed temperature contrast within the regime diagram. To understand the flow field which results from such conditions it is essential to be able to represent the boundaries of the various stationary-state regions, the transitions between them, and particularly the associated hysteresis behavior.

Our aim here is to present a new mathematical setting for the discussion of these experiments, based on René Thom's recently developed "catastrophe theory" (1975), an innovative mathematical language for the description of abrupt changes in behavior. According to this theory, many discontinuous phenomena can be classified (up to arbitrarily close approximation) as one of a finite list of standard behavior types called "elementary catastrophes." The starting assumption of the theory is that certain "control" parameters (directly controllable or at least observable by the scientist) influence other internal "state" parameters

through some equilibrium principle such as the second law of thermodynamics.

In our case, the control parameters will be the temperature contrast and rotation rate, and the states will be certain energies whose values determine the number of waves in the pattern. Let us now concentrate on the control settings at which "behavior" (i.e. equilibrium values of the internal states) jumps discontinuously. Any setting of controls determines a point in "control space," and those control points at which behavior jumps discontinuously are called collectively the "catastrophe set." The theory then asserts that the behavior of the system near any particular point on the catastrophe set must be like one of the elementary catastrophes in the finite list. For the annulus experiments, as a consequence of there being only two control parameters, there are only two elementary catastrophes, the "fold" and the "cusp." For three controls, there are three additional elementary catastrophes, for a total of five; for four controls, there are seven elementary catastrophes altogether. These consequences of the theory are independent of the number of internal state parameters.

The elementary catastrophes may be studied and analyzed geometrically. With the aid of schematic representations, the discontinuous jumping behavior can be visualized, first in the standard models and then in more exact models of the particular situation being studied. In adopting Thom's theory for the representation of the abrupt or "catastrophic" changes in flow-field behavior and associated hysteresis, we hope to provide new insight into the funda-

R. C. Lacher received his B.S., M.A., and Ph.D. (1966) from the University of Georgia, all in mathematics. He has been on Alfred P. Sloan Research Fellow and twice a visitor at the Institute for Advanced Study in Princeton; he is currently professor of mathematics at Florida State University in Tallahassee. Robert McArthur is a graduate student in Florida State's Department of Meteorology. George Buzyna received his B.S. and M.S. from Illinois Institute of Technology and his Ph.D. in 1967 from Yale University, where he studied engineering, applied science, and the physics of fluids. He has done postdoctoral work at Woods Hole and Yale and is currently a Research Associate of the Geophysical Fluid Dynamics Institute at Florida State. The authors wish to thank their colleagues R. Pfeffer and R. Kung, for making their unpublished data available, and the National Science Foundation, the National Oceanic and Atmospheric Administration, and the Office of Naval Research for continuing support. Address: Dr. Lacher, Department of Mathematics, Florida State University, Tallahassee, FL 32306.

mental processes underlying such events.

Although catastrophe theory is used here in the context of laboratory simulations of geophysical flows, it is by no means restricted to such applications. Indeed, Thom's theory can be thought of as a prediction that certain shapes (catastrophes) are the most likely to occur in nature. The manifestation may be in space-time: Thom's original idea was to classify the forms most likely to be observed in early embryonic development. His "controls" were three space coordinates and time; his "states" were all the biochemical variables of the embryo. As we will illustrate here, catastrophes may also be discovered in data. Our presentation of this new application of the theory is intended to draw attention to its potential as an aid both in the investigation of complex data and in the design of future experiments.

Experimental background

Laboratory experiments simulating certain aspects of large-scale atmospheric dynamics have been conducted by numerous investigators over the last twenty-five years (Fultz et al. 1958, 1964; Hide 1958, 1970; Kaiser 1970; Pfeffer et al. 1974). In most of these studies the annulus containing the working fluid, a liquid, was rotated about its vertical axis at a constant rotation rate, Ω , while the inner wall of the annulus was main-

tained at a cold, and the outer wall at a warm, temperature to produce an externally imposed temperature contrast, ΔT . For different values of the control parameters Ω and ΔT the contained fluid will exhibit different flow patterns and different relative balances of fundamental forces driving the flow.

The streak photographs of Figure 1 illustrate some of these flow configurations. The symmetric pattern of (A) is observed at relatively low Ω and high ΔT . The wave patterns shown in (B) and (C) are manifestations of fundamental instabilities of the flow field and occur at higher Ω . The five-wave pattern will occur at a higher Ω with ΔT fixed or at a lower ΔT with Ω fixed. Under appropriate conditions these wavelike flows serve as idealizations of large-scale atmospheric motion and share certain of its properties. The striking resemblance between the idealized laboratory wave pattern and a large-scale atmospheric flow field as represented by a weather chart at a height of 500 mb is shown in Figure 2.

A typical regime diagram schematically representing the results of a flow-field experiment is shown in Figure 3. The transition curves on the boundaries between the regions were obtained by Fultz et al. (1964) in an experiment in which ΔT was increased very slowly and Ω was held constant. For example, as ΔT crosses the 4-3 line in Figure 3, a four-wave flow pattern breaks up and a three-

wave pattern forms. This process of breaking up and reforming is a transient effect and is not represented in the regime diagram.

Hysteresis and intransitive behavior

The phenomenon of hysteresis, a lag in effect when the forces acting on a body are changed, was first observed by Fultz (1958, 1964; Kaiser 1970). When experiments are conducted in which ΔT is changed very slowly, hysteresis is observed in the transitions between adjacent wave patterns. Figure 4 illustrates this effect through an overlay of two regime diagrams using Fultz's 1964 data. As the overlay clearly reveals, there are regions in the regime diagram of a given system in which behavior is bimodal: that is, depending on the history of the control parameters, there are at least two stable fluid-flow configurations for the same external conditions. Such behavior has been described by Lorenz (1967b) as "intransitive." Progress has been made (Lorenz 1962; Cole 1971) in attempting to exhibit this phenomenon in mathematical models based on substantially simplified governing equations of motion.

We suggest an alternative method of representing these experimental results, using Thom's catastrophe theory. The model we propose for the qualitative behavior of annulus experiments is, in a certain sense, the simplest possible model that accounts



Figure 1. Streak photographs illustrate three typical flow patterns in a differentially heated rotating annulus of fluid: (A) symmetric, $\Omega = 1.88$ radians per sec; (B) three-wave, $\Omega = 2.19$ radians per sec; (C) five-wave, $\Omega = 2.57$ radians per sec. All experiments were conducted with

a ΔT of 20° C. In these two-second time exposures the streaks are formed by aluminum flakes suspended in the interior of silicone fluid and represent motion in the upper layers of the fluid. The camera was rotated counterclockwise, with the annulus; the flow and the drift

of the wave pattern were also counterclockwise. The radial lines in the photographs are exterior to the fluid. (Experimental details are the same as in Pfeffer et al. 1974.)

THIS PAGE IS BEST QUALITY PRACTICABLE
FROM COPY FURNISHED TO DDC

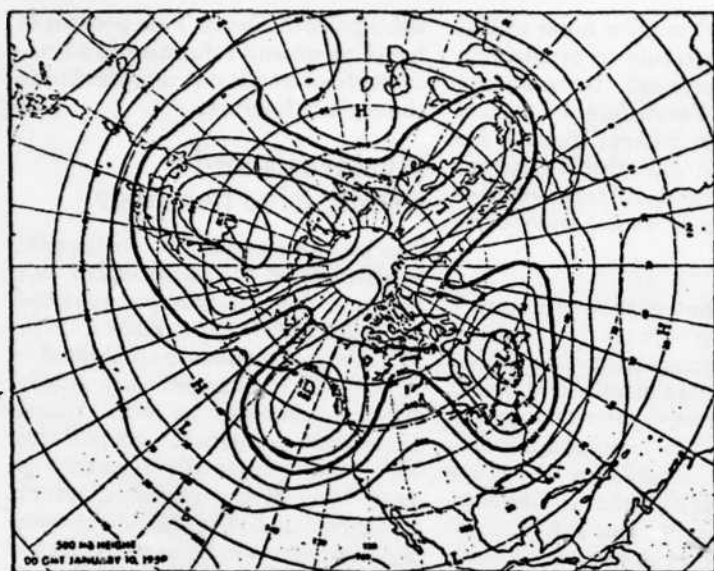
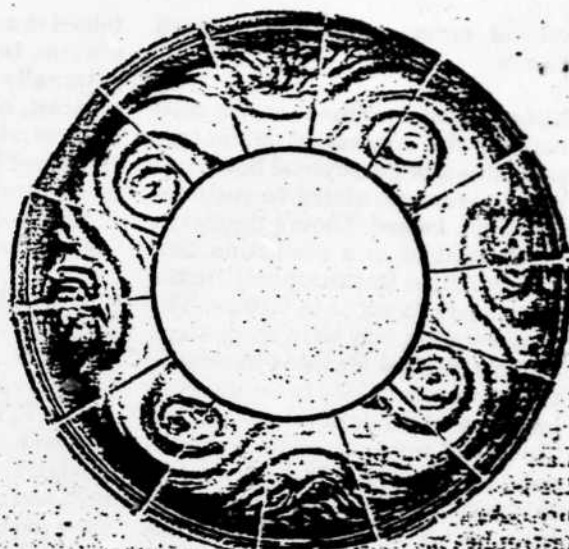


Figure 2. Comparison shows similarities between the global 500 mb pressure pattern in the upper atmosphere of the Northern Hemisphere and a four-wave pattern in the laboratory.



(Laboratory flow conditions were similar to those in Fig. 1, except $\Omega = 1.95$ radians per sec.) In the atmosphere the flow is approximately parallel to the isobars (the flow is to the right,

from high to low pressure), with speed inversely proportional to the spacing. Changes in the wave pattern have a significant effect on large-scale weather and climate.

for the observed hysteresis and intransitivity.

The number of waves of a flow pattern is a convenient means of classi-

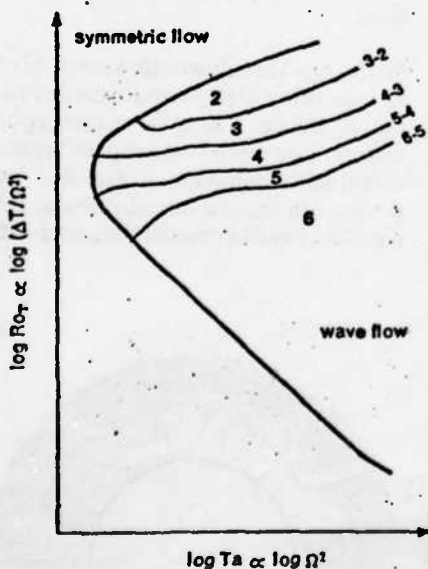


Figure 3. A regime diagram indicates stationary-state flow characteristics in an annulus experiment. Symmetric flow, as in Fig. 1A, occurs when control parameters are to the left of the black line. The black line represents the boundary between the symmetric flow and wave flow regimes, while the colored lines indicate observed boundaries between regions of different dominant wave forms of the flow field. The number marked in each region represents the number of waves apparent in the flow pattern, and the two numbers on the boundary or transition curves between the regions indicate the sequence of the transition. (After Fultz et al. 1964.)

fying flow fields and constructing regime diagrams. An internally measured parameter, however, is better suited to the mathematical modeling to be considered here. The components of an atmospheric energy cycle proposed by Lorenz (1955) have been useful in studying long-term fluid flow both in the atmosphere (Krueger et al. 1965; Winn-Nielson 1967; Oort 1964) and in the annulus (Pfeffer et al. 1974). Lorenz breaks up the usable energy into kinetic and available potential energy, each of which is the sum of a "zonal" and an "eddy" component. The zonal available potential energy is the amount of energy which would exist if the mass field were replaced by its average along latitudinal circles, and the eddy available is the excess of the total available potential energy over its zonal component. Thus the eddy available potential energy is roughly that which can be converted directly into nonsymmetric motion.

The energetics of the annulus experiments is not completely understood. Nevertheless, some generalities are accepted. The total energy of the fluid (or any component of total energy as defined by Lorenz) is a continuous function of time as long as Ω and ΔT are varied continuously. Moreover, the stationary values of some (perhaps all) of these energy components are correlated with wave number, and there is a jump in the stationary value when wave-number transition lines

are crossed in a regime diagram. These last conclusions are borne out for the available potential energy components by experiments recently completed by Buzyna et al. (in prep.). In experiments with many internal thermistor probes (Pfeffer et al. 1974) the components of the available potential energy can be measured. The eddy available potential energy is a particularly sensitive indicator of changes in wave form and hysteresis.

Thus we can construct an energy regime diagram which looks qualitatively like Figure 4; the transition lines now represent discontinuous jumps in energy-stationary values. Our model will offer a means for the representation of such diagrams.

The cusp model

The total energy (or any Lorenz component of energy) of the fluid in a particular annulus experiment can depend only on Ω , ΔT , and time. Letting E denote energy, or mean energy where high-frequency time-dependent behavior at fixed ΔT and Ω is observed, it seems reasonable that E should be a smooth function of these variables for a given set of initial conditions. Thus it seems reasonable to assume that there is a smooth function $f(\Omega, \Delta T, E)$ whose value at a point in $(\Omega, \Delta T, E)$ -space is the tendency of E to increase or decrease

THIS PAGE IS BEST QUALITY PRACTICABLE FROM COPY FURNISHED TO DDC

FROM COPY FILE

at that point. That is, we assume that

$$\dot{E} = f(\Omega, \Delta T, E) \quad (\text{Eq. 1})$$

where the dot indicates differentiation with respect to time ($\dot{E} = dE/dt$). The equilibria of (Eq. 1) must lie on the surface

$$f(\Omega, \Delta T, E) = 0 \quad (\text{Eq. 2})$$

in $(\Omega, \Delta T, E)$ -space; the stable equilibria represent stationary values of energy.

In addition to the rather minimal restrictions made on f in the above paragraph, we make one other, that the model is "generic." This last assumption will be explained in detail below; intuitively, a generic model is one which is given by a potential function on $(\Omega, \Delta T, E)$ -space whose qualitative properties are not changed by small perturbations. Thom's theory, as we will see, implies that the singularities of the model are either folds or cusps.

Focusing attention on one bimodal region of the control plane, the experimental results reviewed above show that the model must have a singularity over that region, and the existence of adjacent unimodal regions rules out a simple fold. We are left with the conclusion that the stationary values of energy must lie on a multicusp surface. Thus Thom's theory argues strongly that a cusp model closely approximates the behavior found in the annulus experiments in a region of the regime diagram containing only one wave-number change. Before pursuing this argument in detail we will explore a qualitative model for the dynamical behavior of E based on the standard or "canonical" cusp surface.

Consider the equation

$$\epsilon \dot{x} = -(x^3 - ax + b) \quad (\text{Eq. 3})$$

We briefly describe the dynamical geometry. Assume $\epsilon > 0$ and a are fixed. Then $\dot{x} = 0$ occurs precisely when (x, b) lies on the locus

$$x^3 - ax + b = 0 \quad (\text{Eq. 4})$$

in the (x, b) -plane (see Fig. 5). Note that (Eq. 4) separates the plane into two connected regions, one in which the expression on the left is positive

and the other in which it is negative. Since $x^3 - ax + b > 0$ for large x , we conclude that $\dot{x} < 0$ throughout the region containing large x ; similarly, $\dot{x} > 0$ throughout the other region. It follows that for constant values of b , the (time) flow lines for the model based on (Eq. 3) are oriented parallel to the x -axis in (b, x) -space with direction as indicated by the arrows in Figure 5.

Allowing a to vary (but keeping $\epsilon > 0$ fixed) we can keep track of the dynamics of (Eq. 3) in (a, b, x) -space. The equilibrium points form a surface (Eq. 4) as shown in Figure 6; this is a "cusp surface." The flow is visualized by gluing together the various vertical (b, x) -planes (Fig. 5). Note that the equilibria in the folded region of the cusp are unstable and therefore are never attained in any physical system. The remainder of the points on the surface represent stable equilibria (rest states) for x . The constant $1/\epsilon$ is a measure of response speed.

Our conclusion above was that the model based on (Eq. 1), near a single bimodal region in $(\Omega, \Delta T)$ -space, could be expected to be the same as the (Eq. 3) model after a change of coordinates. Thus we might suggest the conditions

$$\begin{aligned} \epsilon \dot{x} &= -(x^3 - ax + b) \\ a &= a(\Omega, \Delta T) \\ b &= b(\Omega, \Delta T) \\ E &= E(x) \\ \epsilon &= \text{constant} \quad (\text{Eq. 5}) \end{aligned}$$

as a model of an annulus experiment in which $(\Omega, \Delta T)$ are varied slowly in and near a bimodal region. Certainly this model would account for many of the qualitative aspects of known data. In particular, the hysteresis effect can be visualized by imagining the control parameters (a, b) traveling slowly into the cusp region from one side, passing through the cusp region, and finally moving out on the other side. As (a, b) moves out of the cusp region, the rest state of x "jumps" away from the fold and plunges to the surface again. Traversing the same path in reverse produces a jump in the rest state of x at a different (a, b) coordinate; see paths ABCD and DEFA in Figure 6.

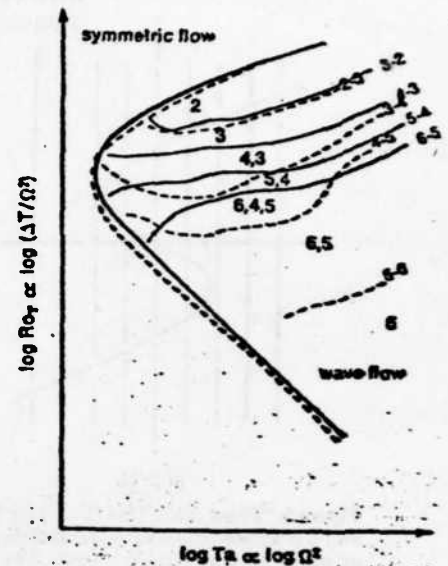


Figure 4. An overlay of two regime diagrams shows hysteresis effects. The solid lines indicate the transitions between wave numbers as ΔT is slowly increased, keeping Ω fixed, and the dashed lines indicate the transitions as ΔT is slowly decreased. Similar results may be obtained by keeping ΔT fixed and slowly varying Ω . The lines shown in color constitute the catastrophe set. (After Fultz et al. 1964.)

Another phenomenon which is easier to represent with this model is the apparent unpredictability and distribution of null experiments within a regime diagram (Hide and Mason 1975). Such experiments consist of rapidly spinning up an annulus to a certain Ω , holding ΔT fixed, and measuring wave number (or energy) after stabilization. Several spinups to the same $(\Omega, \Delta T)$ may produce different wave forms and energy levels. Similarly, we can hold $(\Omega, \Delta T)$ fixed and allow a fluid-flow pattern to stabilize; when the fluid is then stirred with a rod and allowed to restabilize, a different flow pattern may be visible (Hide and Mason 1975). These data are inconsistent with the hypothesis that the stationary value of E is a function of the rest state of the control parameters alone: the stable value of $E(x)$ depends on the approach path to (a, b) in the control plane as well as on (a, b) itself.

Generic models

Assume that C and S are Euclidean spaces (or open subsets of Euclidean spaces), say of dimension m and n respectively, so that a typical point of C is an m -tuple (c_1, \dots, c_m) and a typical point of S is an n -tuple (s_1, \dots, s_n) . Think of C as a space of

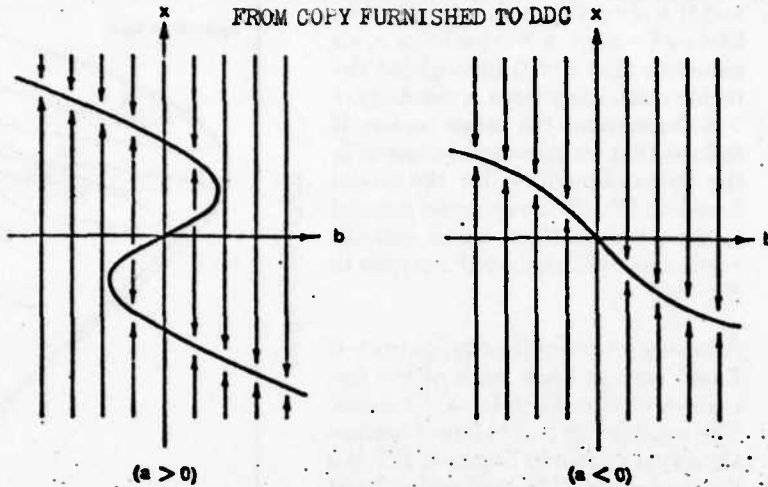


Figure 5. "Phase plane" for (Eq. 3) for fixed ϵ and a is shown. The arrows indicate direction of travel of x as time increases. The curve consists entirely of equilibria (points that do not move as time increases). When $a > 0$, the

equilibria on the inner portion of the curve are unstable (small perturbations from the curve will send x away toward a different portion of the curve). All other equilibria are stable.

"control" variables and S as a space of "state" variables. In the applications above, C is the $(\Omega, \Delta T)$ -plane and S may consist of one (or more) components of the Lorenz energy cycle. The models we consider are of the form

$$\dot{s} = f(c, s)$$

where $f: C \times S \rightarrow S$ is a continuous state-valued function of control and state variables and

$$\dot{s} = \left(\frac{ds_1}{dt}, \dots, \frac{ds_n}{dt} \right)$$

As used above, the word "generic" applied to the model means that

$$f = -\nabla_S F$$

where F is a real-valued function on $C \times S$ (i.e. of control and state variables) with continuous partial derivatives of all orders, and that F is structurally stable in the C^∞ -topology. The partial gradient $\nabla_S F$ is

$$\left(\frac{\partial F}{\partial s_1}, \dots, \frac{\partial F}{\partial s_n} \right)$$

We will explain structural stability after establishing some notation.

For any real-valued F on $C \times S$, let M_F be the equilibrium points of the associated vector field, i.e. M_F consists of those points (c, s) in $C \times S$ at which $\nabla_S F$ is zero. The projection $\pi: C \times S \rightarrow C$ restricts to a mapping $\pi_F:$

$M_F \rightarrow C$. Now, F is structurally stable if, given a point p on M_F , there is some $\epsilon > 0$ and k such that whenever G and all partials of G of order $\leq k$ are within ϵ of those of F , then there are smooth local coordinate changes ϕ around p in $C \times S$ and ψ around $\pi(p)$ in C such that $\pi\phi = \psi\pi$ and $\phi(M_F) = M_G$ (near p). To put it another way, F is stable if small perturbations of F do not change the qualitative behavior of the equilibria of its derived model.

Theorem 1 (Whitney, Thom, Mather). If the dimension of C is 5 or less, the structurally stable functions on $C \times S$ form an open, dense set in the C^∞ -topology—i.e. any small smooth perturbation of a stable function is stable (this is the definition of stability!), and any function with k continuous derivatives can be C^k -approximated by a stable function.

Thus if a model f of any natural phenomenon is given by a potential function F , the modeler is forced to assume F is structurally stable. To begin with, almost all potential functions are structurally stable; and having an unstable potential function is equivalent to being unmodelable, since any error in constructing the model, no matter how minute, would produce qualitatively incorrect behavior.

Whether a model should be given by a potential function is another question. In many instances, such a po-

tential function is a probability distribution which wants to be maximized or an energy function which wants to be minimized (Zeeman 1975, 1976). In the situation we are considering, the potential function might be thought of as the "energy transport rate" function: the fluid in an annulus experiment tries to optimize the transport of heat energy between the outer and inner walls of the annulus. It is worth emphasizing, however, that the potential function need not have direct physical significance: in catastrophe theory, its role may be simply to govern the associated differential equations.

Theorem 1 gives the justification for assuming that our model is generic. The next theorem tells how this assumption leads to the conclusions reached earlier in the paper. For our purposes here, we can get by with the following concept of "singularity." Assume f is a generic model with associated function $F: C \times S \rightarrow \text{real numbers}$. A point p on M_F is regular if there is some neighborhood U of p on M_F such that π_F is one-to-one on U . (The real definition is based on the fact that M_F is a differentiable manifold: in this context, a regular point of π_F is a point p at which the intrinsic derivative $D\pi_F$ is nonsingular.) Otherwise, p is a singular point, or a singularity of π_F . Singularities of π_F are important for the model

$$\dot{s} = -\nabla_S F$$

because they represent points on the equilibrium surface where bifurcation is possible as control parameters are slowly changed. Conversely, if p is a regular point on M_F , and if U is the associated neighborhood, then moving control parameters about in $\pi(U)$ will move equilibrium states about in U in a totally predictable way, because $\pi|U: U \rightarrow \pi(U)$ is invertible. The dynamics of the model keep rest states on the equilibrium surface whenever possible. Thom refers to the image of the singularities under π as the "catastrophe set." Thus in the canonical cusp discussed above, the catastrophe set is the V-shaped curve $27b^2 = 4a^3$ in the control plane shown in Figure 6.

Theorem 2 (Thom). If F is structurally stable, then M_F is a manifold of the same dimension as C and any singularity of π_F is, up to smooth changes of coordinates, an "elemen-

ary catastrophe." The number of types of elementary catastrophes depends only on the dimension of C . If the dimension of C is less than 5, this number is finite, as given here:

dim C	1	2	3	4	5	6
no. of elementary catastrophes	1	2	5	7	11	∞

Thom goes on to classify the elementary catastrophes for $\dim C \leq 4$. In particular, when $\dim C = 2$, the only two possible types are folds and cusps. The canonical cusp is given by the function

$$F(a, b, x) = \frac{x^4}{4} - a \frac{x^2}{2} + bx$$

on $C \times S = [(a, b)\text{-space}] \times [x\text{-space}] = (a, b, x)\text{-space}$. The behavior of the derived model

$$\dot{x} = -\nabla_S F = -(x^3 - ax + b)$$

was described in detail above. The simpler fold is given by

$$F(a, x) = \frac{x^3}{3} - ax$$

The reader may enjoy exploring its derived model. See Thom (1975) or Bröcker (1975) for descriptions of the other elementary catastrophes.

When S has many variables, say s_1, \dots, s_n , the canonical cusp is given by

$$G(a, b, s_1, \dots, s_n) = \frac{s_1^4}{4} - a \frac{s_1^2}{2} + bs_1 + \frac{s_2^2}{2} + \dots + \frac{s_n^2}{2}$$

and the derived model is

$$\begin{aligned} \dot{s}_1 &= -(s_1^3 - as_1 + b) \\ \dot{s}_2 &= -s_2 \\ &\dots \\ \dot{s}_n &= -s_n \end{aligned}$$

i.e. motion is linear in all but the first variable. Thus according to Thom's theorem, no matter how many "state" variables we choose to observe in the

annulus experiments, it is always at least theoretically possible to change coordinates smoothly in and near a given bimodal region in such a way that afterward one variable exhibits the pathological behavior of the model while the other variables behave linearly. Some energy component or other internal variable must behave according to the model based on (Eq. 5); which variable does so may change from cusp to cusp. A fortunate property of the annulus experiments is that one energy, the eddy available potential energy, can represent the entire family of cusps.

The regime diagram

The mathematical theory we have presented, together with the experimental evidence, leads to the inescapable conclusion that the behavior of an annulus experiment is closely approximated by a model $\dot{E} = f(\Omega, \Delta T, E)$ where $f = -\nabla_E F$, F is structurally stable, and π_F has a cusp over each of the lines of hysteresis in the control plane (regime diagram), as long as Ω and ΔT are varied slowly and represent the only control parameters. In the context of this theory a schematic representation of the behavior observed in Figure 4 is shown in Figure 7. Note that as a consequence of the theory, each hysteresis region in the control plane must converge to a single point. This behavior is suggested but not represented explicitly in the superimposed data of Figure 4. Subsequent very careful experimental work by Kaiser (1970) has revealed that the transition curves on both increasing and decreasing ΔT do indeed emanate from the same point for a given hysteresis region. Additional discoveries by Kaiser deal with further details of the transition near the symmetric region and can easily be incorporated in the surface represented in Figure 7.

As we proceed deeper into the wave regime (i.e. farther from the symmetric regime boundaries) the structure becomes more complex. We begin to encounter multiple folding of the surface, as demonstrated by the sheets of wave numbers 4, 5, and 6 in Figure 7. We have already seen how a simple fold can give rise to bimodal behavior, and multiple folding increases the number of energy-stationary values (or flow patterns) possible at a given point in control

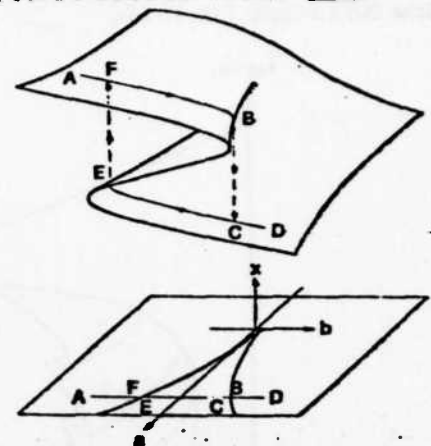


Figure 6. The diagram shows "phase space" for (Eq. 3) for fixed a . Each plane $a = \text{constant}$ is one of the planes represented in Fig. 5. The time-flow lines are not indicated here, but they are the same as those of Fig. 5. Motion of x is in the vertical direction toward the surface, except over the cusp region where motion is away from the inner sheet and toward the outer sheets. The surface itself is composed of equilibrium points, with the inner portion of the cusp representing unstable equilibria and the rest of the surface representing stable equilibria. The V-shaped curve shown in color constitutes the catastrophe set.

parameter space, as is also observed in annulus experiments (Hide and Mason 1975). When increased layering is combined with close packing of sheets, ever-present perturbations may "bump" an energy state from one stable attracting layer past a neighboring unstable layer, at which time the dynamics would shift the energy state to a different attracting layer. The possibility of such "bumping" may give rise to what we might call "wave-number vacillation," where the flow would be characterized by different wave forms at different times but at the same value in the control plane.

As we proceed farther yet into the wave regime it will no longer be possible to represent the flow field in terms of single wave numbers, as in the data for Figures 3 and 4. The flow-field configuration becomes more complex and requires an increasing number of modes for its description. As turbulence is approached and encountered it becomes increasingly necessary to characterize the flow in terms of a spectral energy distribution. As such complexities arise, it might be necessary to consider individual mode energies separately or all together as the variables in a multidimensional-state space.

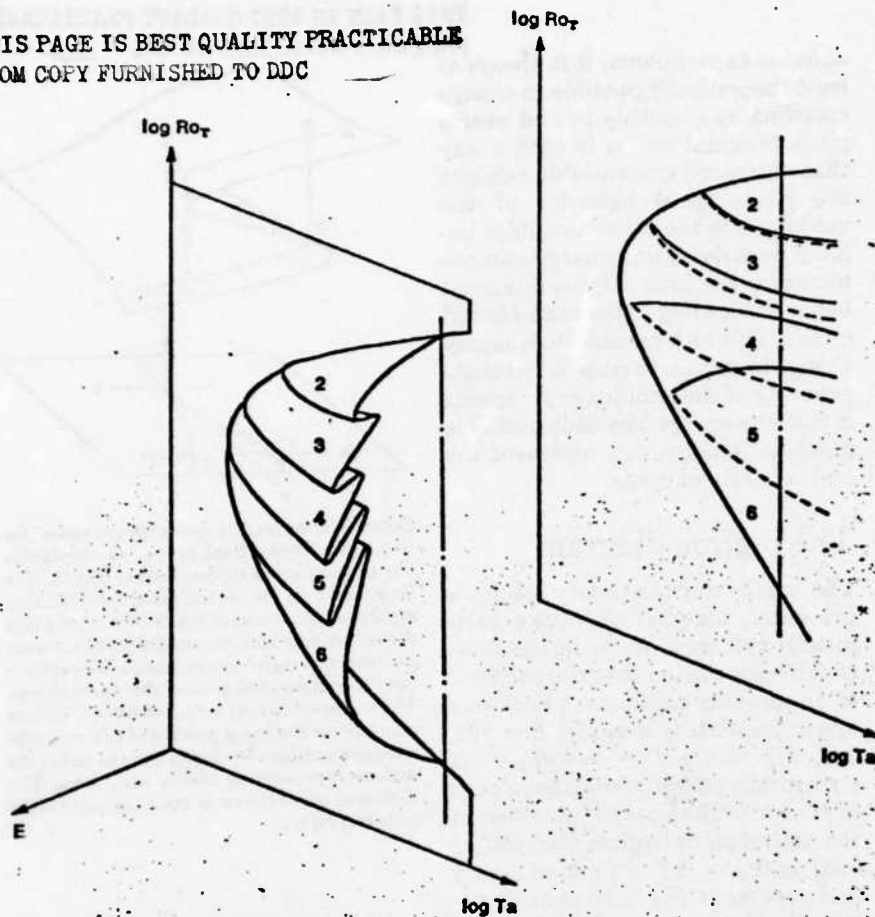


Figure 7. A schematic equilibrium surface represents the experimental results shown in Fig. 4. The colored solid and dashed lines outlining the wave-flow pattern constitute the catastrophe set of the model. The numbers on the surface indicate the wave pattern observed when E lies on that portion of the surface. (E

can represent the eddy available potential energy or the thermal variance of the flow field.) Behavior near each cusp is similar to that of the simpler model discussed in Fig. 6. Experimental results are not accurate enough to determine the slope of the curves shown in color as they approach the cusp point.

Quantitative modeling

For quantitative purposes we need to know the function f with reasonable precision. Of course, one way of obtaining f is to derive it from basic physical principles. Another possibility is to derive F from some basic energy-minimizing principle or from thermodynamics. The latter possibility seems to warrant further study. Completion of such a program would yield a quantitative model that is mathematically and physically sound in the traditional sense.

What we have done thus far is to build a qualitative model that is mathematically sound, has clearly and simply stated assumptions, and incorporates well-established empirical evidence. In the absence of a deduced quantitative model, we could combine our deduced qualitative model with experimental data and

induce a quantitative model. (We refer to such a procedure as "calibration" of the fast dynamic.) A careful calibration might be useful in computer simulations of annulus experiments, especially in the "dynamic case" described below.

Thus far our discussion has been limited to static models: those in which control parameters are varied very slowly so that the system can retain, or quickly return to, its state of equilibrium. Another interesting situation is one in which control parameters are varied on a time scale that interacts with characteristic internal time scales of the physical system. A problem of this sort is posed by laboratory simulation of certain aspects of large-scale atmospheric seasonal and climatic variability. In this case ΔT is varied sinusoidally at a fixed frequency while Ω is kept constant. Before

modeling such behavior it is necessary to consider and clearly define all characteristic time scales of the problem, both in the laboratory and in the proposed mathematical setting. Adding periodic dynamics to ΔT in the static model introduces a second time scale that must be compared with the response time scale of the equation $\dot{E} = f(\Omega, \Delta T, E)$. (In the canonical cusp, when dynamic control parameters are introduced, $1/\epsilon$ is a measure of the time response of the system; other characteristic times are determined by the control parameters.)

In the laboratory experiment there are at least three characteristic time scales that must be considered: (1) the period of the dominant physical mechanism, such as amplitude vacillation (Pfeffer and Chiang 1967) or tilted trough vacillation (Fultz et al. 1958); (2) "response" time (i.e. an e-folding time required to reattain equilibrium after a change in control parameters); and (3) the external forcing period. For example, in a particular annulus (Buzyna et al., in prep.) a characteristic time in category (1), due to amplitude vacillation, is 200 sec. In the same annulus the thermal response time is approximately 1,000 sec. In deciding what period to assign to ΔT , we are most interested in numbers which yield thermal lags of between 0.085 and 0.17 cycles of ΔT (one to two "months"). In this example, forcing periods of one to two hours result in lag times of 660–860 sec, or 0.18 to 0.12 of the period, respectively. Thus the action (2) will be at least four times as fast as (3).

In modeling the static case we have filtered out the high-frequency time dependence (1) by considering mean value of energy over a period of vacillation. These mean energies are the energies correlated with wave number, as discussed earlier. In the dynamic case, it is again these mean energies which reflect the flow-pattern behavior. As long as the time scale (3) is considerably slower than (2), it seems reasonable to build a dynamic model by simply adding periodic forcing to ΔT in the static model. We hope to carry out such a program in the future. (Compare Zeeman 1972.)

In this connection it is interesting to note results obtained by Buzyna et al.

In recent experiments with periodic variation of ΔT (in prep.). They found that when the ratio of thermal lag time to cycle time is 0.02, the behavior can be represented accurately by a static cusp model. However, when this ratio is increased to 0.12, the flow begins to show a large latitude in the point of transition between different flow patterns in the hysteresis region, and thus in a sense the flow pattern appears "unpredictable" at a given point with respect to the behavior observed with a much lower value of the time ratio. It appears that above a certain value of the ratio the flow is able to undergo a transition in wave form anywhere in the bimodal region. In the context of the theory, the time-flow lines should reflect such behavior and represent both the history and the probable point of wave-form transition.

Higher dimensional problems

In a situation where intransitive behavior is encountered but experimental evidence does not conform with a simple cusp or fold model, yet there is nevertheless reason to believe a generic model exists, one is forced to conclude that some unnoticed external parameter is operative. Conversely, if we introduce another external control parameter, say viscosity, a three-dimensional control space must be considered: there is now the possibility of three additional singularity types. These new catastrophes will be composed of families of cusps together with a new point at which pathology is essentially three-dimensional. (In much the same way, a cusp is composed of a family of folds together with a point at which pathology is essentially two-dimensional.)

This more complicated situation will require careful study to decide which, if any, of the essentially three-dimensional catastrophes is inherent in the energy dynamics. (Since the cusp is the only essentially two-dimensional catastrophe, this question almost answers itself in the case of a two-dimensional control plane.) Obviously, viscosity is difficult to vary continuously and slowly while maintaining constant (Ω , ΔT), and thus data pertinent to this three-dimensional case will be difficult to obtain.

In a situation where there are complex data to be analyzed, Thom's extremely flexible theory, with its prediction that only certain special types of catastrophes are likely to occur, is an invaluable tool. In employing this theory to construct a model that accounts for the phenomena of hysteresis and intransitivity in circulation flow patterns, we have demonstrated only one of its possible uses. Thom's theory is widely applicable, and allows new insight in constructing global dynamical models from experimental data as well as pointing the way to the design of more effective experiments.

References

- Bröcker, T. H. 1975. *Differential Germs and Catastrophes*. Cambridge: London Math. Soc. Lect. Notes, Vol. 17.
- Buzyna, G., R. L. Pfeffer, and R. Kung. In prep. Response of a thermally driven rotating fluid to periodic variations in the imposed temperature contrast and possible implications to seasonal and climatic variability.
- Cole, R. J. 1971. Hysteresis effects in a differentially heated rotating fluid annulus. *Quart. J. Roy. Meteor. Soc.* 97:506-18.
- Fultz, D., J. Kaiser, M. Fain, R. Kaylor, and J. Weil. 1964. Experimental investigations of the spectrum of thermal convective motions in a rotating annulus. In *Final Report, Research on Hydrodynamic Analogues of Large Scale Meteorological Phenomena*. AFCRL-64-382, Contract AF 19(604)-8361, April. Bedford, MA: U.S. Air Force Cambridge Research Laboratories.
- Fultz, D., R. Loy, G. Owens, W. Bohan, R. Taylor, and J. Weil. 1958. Studies of thermal convection in a rotating cylinder with some implications for large-scale atmospheric motions. *Meteor. Mon.* 4:77-101.
- Hide, R. 1958. An experimental study of thermal convection. *Phil. Trans. Roy. Soc. A* 250:441-78.
- . 1970. Some laboratory experiments on free thermal convection in a rotating fluid subject to horizontal temperature gradient and their relation to the theory of global atmospheric circulation. In *The Global Circulation of the Atmosphere*, ed. G. A. Corby, pp. 196-221. London: Roy. Meteor. Soc.
- Hide, R., and P. J. Mason. 1975. Sloping convection in a rotating fluid. *Adv. in Physics* 24: 47-160.
- Kaiser, J. A. C. 1970. Rotating deep annulus convection. Part 2. Wave instabilities, vertical stratification, and associated theories. *Tellus* 22:275-87.
- Krueger, A. F., J. S. Winston, and P. A. Haines. 1965. Computations of atmospheric energy and its transformations for a recent five-year period. *Mon. Weather Rev.* 93:227-33.
- Lorenz, E. N. 1955. Available potential energy and the maintenance of the general circulation. *Tellus* 7: 157-67.
- . 1962. Simplified dynamic equations applied to the rotating basin experiments. *J. Atmosph. Sci.* 19:39-51.
- . 1967. *The Nature and Theory of the General Circulation of the Atmosphere*. Geneva: World Meteor. Organ. Publ. No. 218.
- . 1967b. Climatic determinism. *Meteor. Mon.* 8:1-3.
- Oort, A. H. 1964. On estimates of the atmospheric energy cycle. *Mon. Weather Rev.* 22:483-93.
- Pfeffer, R., and Y. Chiang. 1967. Two kinds of vacillation in rotating laboratory experiments. *Mon. Weather Rev.* 95:75-82.
- Pfeffer, R., G. Buzyna, and W. W. Fowles. 1974. Synoptic features and energetics of wave-amplitude vacillation in a rotating, differentially heated fluid. *J. Atmosph. Sci.* 31: 622-45.
- Thom, R. 1975. *Structural Stability and Morphogenesis*. Reading, MA: W. A. Benjamin, Inc.
- Winn-Nielsen, A. 1967. On the annual variation and spectral distribution of atmospheric energy. *Tellus* 19:540-60.
- Zeeman, E. C. Geometry of catastrophe. *London Times Literary Supplement*, 10 Dec. 1971.
- . 1972. Differential equations for heartbeat and nerve impulses. *Towards a Theoretical Biology*, Vol. 4, ed. C. H. Waddington, pp. 8-67. Edinburgh Univ. Press.
- . 1975. Levels of structure in catastrophe theory as illustrated by applications in the social and biological sciences. In *Proc. Int. Cong. Math.*, Vol. 2, pp. 533-45. Vancouver: Canadian Math. Congress.
- . 1976. Catastrophe theory. *Sci. Am.* 234:65-83.

THIS PAGE IS BEST QUALITY PRACTICABLE
FROM COPY FURNISHED TO DDG

Abstract

Rotating annulus experiments are described in which the imposed thermal forcing is varied periodically by means of cyclic variations of the cold inner-bath temperature. In the way of background, the results of conventional annulus experiments, in which the imposed temperature contrast is not varied, and of hysteresis experiments, in which the imposed temperature contrast is varied slowly enough to be considered quasi-static, are reviewed. It is found that, in the region of dimensionless-parameter space in which our experiments were conducted, the flow configuration in conventional and hysteresis experiments is *determinate* in the sense that it depends only upon the point in dimensionless-parameter space at which the experiment is conducted and the direction from which this point is approached. The flow configuration in experiments in which the imposed temperature contrast is varied in a cyclic fashion is found to be *indeterminate* in the sense that it changes from one state to another sporadically and cannot be predicted solely as a function of 'season'.

Cyclic Variations of the Imposed Temperature
Contrast in a Thermally Driven Rotating Annulus of Fluid¹

by

George Buzyna, Richard L. Pfeffer*, and Robin Kung

Geophysical Fluid Dynamics Institute
and
Department of Meteorology*
Florida State University

ACCESSION for	
NTIS	White Section <input checked="" type="checkbox"/>
DDC	Diff Section <input type="checkbox"/>
UNANNOUNCED	<input type="checkbox"/>
JUSTIFICATION	<i>Per letter</i>
<i>on file</i>	
<i>see sheet R-78-1139</i>	
DISTRIBUTION/AVAILABILITY CODES	
Dist.	AVAIL. and/or SPECIAL
A	

¹Contribution number 000 of the Geophysical Fluid Dynamics Institute, Florida State University.

**DAT
FILM**